Ann. Geophys., 29, 299–319, 2011
www.ann-geophys.net/29/299/2011/
doi:10.5194/angeo-29-299-2011

Annales Geophysicae

EISCAT-Cluster observations of quiet-time near-Earth magnetotail fast flows and their signatures in the ionosphere

T. Pitkänen[1], **A. T. Aikio**[1], **O. Amm**[2], **K. Kauristie**[2], **H. Nilsson**[3], **and K. U. Kaila**[1]

[1]Department of Physics, University of Oulu, P.O. Box 3000, 90014, Finland
[2]Finnish Meteorological Institute, Helsinki, Finland
[3]Swedish Institute of Space Physics, Kiruna, Sweden

Received: 29 October 2010 – Revised: 31 January 2011 – Accepted: 2 February 2011 – Published: 10 February 2011

Abstract. We report observations of a sequence of quiet-time Earthward bursty bulk flows (BBFs) measured by the Cluster spacecraft in the near-tail plasma sheet ($X_{GSM} \sim -12$ to -14 R_E) in the evening sector, and by simultaneous high-resolution measurements in the northern conjugate ionosphere by the EISCAT radars, a MIRACLE all-sky camera and magnetometers, as well as a meridian-scanning photometer (MSP) in the Scandinavian sector on 17 October 2005.

The BBFs at Cluster show signatures that are consistent with the plasma "bubble" model (Chen and Wolf, 1993, 1999), e.g. deflection and compression of the ambient plasma in front of the Earthward moving bubble, magnetic signatures of a flow shear region, and the proper flows inside the bubble. In addition, clear signatures of tailward return flows around the edges of the bubble can be identified. The duskside return flows are associated with significant decrease in plasma density, giving support to the recent suggestion by Walsh et al. (2009) of formation of a depleted wake. However, the same feature is not seen for the dawnside return flows, but rather an increase in density.

In the ionosphere, EISCAT and optical measurements show that each of the studied BBFs is associated with an auroral streamer that starts from the vicinity of the polar cap boundary, intrudes equatorward, brakes at 68–70° aacgm MLAT and drifts westward along the proton oval. Within the streamer itself and poleward of it, the ionospheric plasma flow has an equatorward component, which is the ionospheric manifestation of the Earthward BBF channel. A sharp velocity shear appears at the equatorward edge of a streamer. We suggest that each BBF creates a local velocity shear in the ionosphere, in which the plasma flow poleward of and inside the streamer is in the direction of the streamer and southeastward. A northwestward return flow is located on the equatorward side. The return flow is associated with decreased plasma densities both in the ionosphere and in the magnetosphere as measured by EISCAT and Cluster, respectively. In summary, we present the first simultaneous high-resolution observations of BBF return flows both in the plasma sheet and in the ionosphere, and those are in accordance with the bubble model. The results apply for the duskside return flows, but the manifestation of dawnside return flows in the ionosphere requires further studies.

Finally, EISCAT measurements indicate increased nightside reconnection rate during the ∼35-min period of BBFs. We suggest that the observed temporal event of IMF rotation to a more southward direction produces enhanced open flux transport to the nightside magnetotail, and consequently, the nightside reconnection rate is increased.

Keywords. Ionosphere (Polar ionosphere) – Magnetospheric physics (Auroral phenomena; Magnetosphere-ionosphere interactions)

1 Introduction

Earthward plasma and magnetic flux transport in the magnetotail plasma sheet has been long known to be dominated by transient fast flows in ambient plasma convection (Baumjohann et al., 1989, 1990). The fast flows have been observed to appear as bursty bulk flow events on a time scale of 10-min (BBFs), a bulk flow being composed of individual flow bursts of an order of a minute time scale (Angelopoulos et al., 1992, 1994). The peak velocities of flow bursts are about one magnitude above the average convection velocities and they are often associated with magnetic perturbations, which have been interpreted as the signature of a magnetic flux rope structure embedded into the flow burst (Slavin et al., 2003; Henderson et al., 2006). BBFs are concluded to be

Correspondence to: T. Pitkänen
(timo.pitkanen@oulu.fi)

narrow elongated structures: the characteristic cross-tail extent of BBFs has been estimated to be ∼1–4 R_E across the tail (Sergeev et al., 1996; Angelopoulos et al., 1997; Sergeev et al., 2000; Nakamura et al., 2001a, 2004).

Currently, the most potential theoretical description to explain the main characteristics of a BBF is the bubble model (Chen and Wolf, 1993, 1999). A bubble represents depleted flux tubes that are propelled Earthwards by the interchange instability rising due to the decreased cross-tail current across the flux tubes. The flow shear between the moving bubble and its surroundings creates field-aligned currents on the edges of the bubble, which flow into the ionosphere on the dawnside and out of the ionosphere on the duskside of the bubble (see e.g. Snekvik et al., 2007).

In general, magnetospheric observations support the bubble model. Underpopulated Earthward plasma flows, dipolarization and field-aligned currents have been reported by several authors, e.g. Sergeev et al. (1996, 2000) and Nakamura et al. (2001a,b, 2005). In addition, tailward flows sometimes observed in association with Earthward flow bursts have been suggested to represent the return flows expected to be found around the flanks of a bubble (Kauristie et al., 2000). These return flows are also seen in simulations (Birn et al., 2004), and recently they have been reported by direct observations in the magnetotail (Walsh et al., 2009).

In the ionosphere, BBFs have been found to be associated with narrow, mainly north-south aligned equatorward extending auroral forms called auroral streamers (e.g. Henderson et al., 1998; Sergeev et al., 1999, 2000; Zesta et al., 2000), or local transient activations of aurora (Nakamura et al., 2001a). Both forms initiate at the poleward boundary of the auroral oval and they have been collectively called poleward boundary intensifications (PBIs) (Lyons et al., 1999). Some observations support the idea of PBIs corresponding to the ionospheric counterpart of the upward field-aligned current flowing at the duskside edge of BBFs (e.g. Amm et al., 1999; Sergeev et al., 2000; Nakamura et al., 2001b). Multiple equatorward extending PBIs can occur in a longitudinal direction within the nightside auroral oval suggesting that many fast flow channels may exist over the width of the plasma sheet (Zesta et al., 2006).

The bubble model imposes an ionospheric plasma convection pattern where the ionospheric plasma flow corresponding to the Earthward flow in the magnetosphere is roughly equatorwards and the return flows around the field-aligned currents are polewards, under assumption that there are no significant potential drops along the magnetic field lines. However, in the case of parallel potential drops, the ionospheric convection pattern may be decoupled from the magnetospheric one. Sergeev et al. (2004) were able to associate auroral streamers seen in Polar UVI images in the Northern Hemisphere with the equatorward convection jets in the conjugate Southern Hemisphere extracted from the DMSP satellite data. Grocott et al. (2004) and Nakamura et al. (2005) presented observations by the coherent HF CUTLASS radar of the SuperDARN network that showed localized equatorward convection flow enhancement associated with a bursty bulk flow event.

Senior et al. (2002) reported SuperDARN observations of strong westward convection bursts equatorward of or within a narrow east-west oriented auroral arc in the evening sector. They mapped the flow bursts to the central plasma sheet close to its border. Conjugate DMSP data suggested low conductivity within the region of fast convection. Zou et al. (2009) showed two flow burst events observed by the Poker Flat incoherent scatter radar (PFISR) in the pre-midnight auroral zone that were associated with east-west-oriented PBIs (auroral structures). The flows were found to be associated with low conductivity regions seen in the measured electron densities. Zou et al. proposed that the east-west-oriented PBIs have an extended structure in the tailward direction within the plasma sheet, and that the bursts were flow enhancements superimposed on the background convection flows. Both Senior et al. and Zou et al. suggested the observed enhanced ionospheric plasma flows to be related to ionospheric counterpart flows of BBFs.

The actual processes behind the generation of BBFs are not yet understood, but most probably they are created by reconnection in the magnetotail. E.g. de la Beaujardiere et al. (1994) observed enhanced equatorward plasma flows in the ionosphere in association with arc intensifications (PBIs) at the poleward auroral boundary and interpreted them as the signature of abrupt, localized increases in the reconnection rate. Hubert et al. (2007) analyzed the relation between flux closure and auroral streamer formation in several cases and found that appearance of streamers was associated with intensified reconnection rate, consistent with earlier suggestion by Hubert et al. (2006) that PBIs are related to flux closure. Recently, Pitkänen et al. (2009a,b) showed a direct correlation between PBIs and intensifications in the reconnection electric field, suggesting that the PBIs are a consequence of temporarily enhanced longitudinally localized magnetic flux closure in the magnetotail. However, they all lacked simultaneous in situ satellite measurements of associated plasma flow bursts in the magnetotail.

In this paper, we analyze observations of BBFs measured by the Cluster spacecraft in the magnetotail together with simultaneous ionospheric measurements by a set of ground-based instruments including EISCAT incoherent scatter radars, MIRACLE magnetometers and an all-sky camera as well as a meridian-scanning photometer. The observations of the event are presented in Sect. 2, the results are discussed in Sect. 3, and a summary and conclusions are finally given in Sect. 4.

2 Observations

2.1 Overview

The observations were made on 17 October 2005 during the annual Finnish EISCAT measurement campaign. The event has also been included in the list of bursty bulk flow events collected by Juusola et al. (2009) for a study of the relationship between ionospheric equivalent currents and BBFs.

Throughout this study, the **g**eocentric **s**olar **m**agnetic (GSM) coordinate system is used for the solar wind and magnetospheric data. To present the ionospheric measurements, we use the **a**ltitude **a**djusted **c**orrected **g**eo**m**agnetic (aacgm) coordinate system (Baker and Wing, 1989). In aacgm any two points connected by a magnetic field line have the same coordinates.

Figure 1 shows solar wind and geomagnetic conditions for the period of 16:00–21:00 UT. Top panel shows the IMF components measured by the Magnetic Field Investigation (MFI) instrument (Lepping et al., 1995) onboard the WIND spacecraft ($X_{GSM} \sim 197\ R_E$). The data are 1-min OMNI data, so the solar wind parameters have been propagated to the magnetospheric bow shock nose ($X_{GSM} \sim 14\ R_E$). The time interval until 20:10 UT is characterized by negative B_z and positive B_y IMF components, excluding a period between 17:50 and 19:10 UT, during which rotations of IMF took place. The IMF magnitude stayed constant (5 nT) during the whole 5-h interval.

The second panel shows the solar wind speed (blue) and dynamic pressure (black) obtained by the Solar Wind Experiment (SWE) instrument (Ogilvie et al., 1995). Relatively low values were recorded for the both quantities. The first IMF rotation that occurred 17:50–18:16 UT was associated with a small disturbance seen as a weak enhancement in the solar wind flow speed and a neglectable pulse in the dynamic pressure.

The auroral electrojet indices in the third panel of Fig. 1 show that the geomagnetic activity was low and after 17:00 UT the conditions can be characterized as quiet. Minor increase can be seen after 18:10 UT. However, before the time interval shown here, between 11:30–15:45 UT, the AE index showed continuous activity with a maximum value of 900 nT (data not shown).

The bottom panel shows the east-west equivalent currents calculated from the north-south MIRACLE magnetometer chain data by using the 1-D upward continuation by Vanhamäki et al. (2003). The black curve marks the polar cap boundary estimated from the EISCAT data (see explanation in Sect. 2.3). The magnitudes of the local equivalent currents in the Scandinavian sector mimic the behaviour of the global AE index. In addition, the magnetic Harang discontinuity, i.e. westward electrojet flowing on the poleward side of the eastward electrojet, appears in the equivalent currents 18:00–20:20 UT. After 18:00 UT, the polar cap boundary is located close to the poleward edge of the westward electrojet, a feature that is typical to the nightside region of the westward electrojet (e.g. Aikio et al., 2006, 2008).

These observations show that quiet-time conditions were prevailing in the near-Earth space during the period of interest, 18:00–19:00 UT.

During that period the four Cluster spacecraft (referred hereafter by C1, C2, C3 and C4) were in a tail conjunction with the Scandinavian sector. Figure 2 shows the Cluster positions in the magnetosphere in the GSM coordinate system. The satellites were located close to $Z_{GSM} = 0$ at a distance of -12 to $-14\ R_E$ in X_{GSM} in the near-Earth tail and in the dusk sector (C1: $[-13.9,\ 8.0,\ -0.8]\ R_E$ at 18:00 UT). The satellites were flying antisunwards, and towards dusk. The spacecraft were in the "multiscale" constellation in which C1, C2 and C3 have a larger separation ($\sim$10 000 km) and C4 follows C3 by a shorter distance ($\sim$1000 km).

During the Cluster tail conjunction there were several ground-based instruments monitoring the conjugate ionosphere above the Northern Fennoscandia (Fig. 3). The EISCAT VHF incoherent scatter radar near Tromsø was looking at a low elevation (30°) towards geographic north (azimuth 359.5°) and the EISCAT ESR 32 m antenna on Svalbard was looking at a low elevation (32.4°) geographically southwards (azimuth 168.35°). In addition, the ESR 42m antenna on Svalbard was measuring field-aligned (azimuth 182.1°, elevation 81.6°).

Magnetometer stations of the MIRACLE network (blue dots in Fig. 3) were monitoring the geomagnetic field and an all-sky camera located at Kevo (KEV ASC) was making optical measurements. The field of view (f-o-v) of the ASC corresponding to an altitude of 110 km is marked as a black circle in Fig. 3. In addition, a meridian-scanning photometer by University of Oulu was operating at Kilpisjärvi (KIL MSP, green dashed line) on the southwestern part of the f-o-v of the KEV ASC.

The ionospheric footpoints of the Cluster satellites mapped using the T96 magnetic field model (Tsyganenko and Stern, 1996) are marked by dashed lines. As an input to the T96 model, we used the average solar wind data from the period 16:10–17:50 UT preceding the first IMF rotation. The squares indicate the Cluster footpoint locations at 18:00 UT. During 18:00–19:00 UT the Cluster ionospheric footpoints moved along almost constant latitudes from east to west across the EISCAT radar beams between 68° and 70° MLAT.

2.2 Cluster data

Cluster observations were used to identify BBFs. In this study, we use particle data from the Hot Ion Analyzer (HIA) and from the COmposition DIstribution Function (CODIF) detectors of the Cluster Ion Spectrometry (CIS) instrument (Rème et al., 2001), as well as magnetic field data from the FluxGate Magnetometer experiment (FGM) (Balogh et al., 2001) on board the satellites. Unfortunately, HIA data were

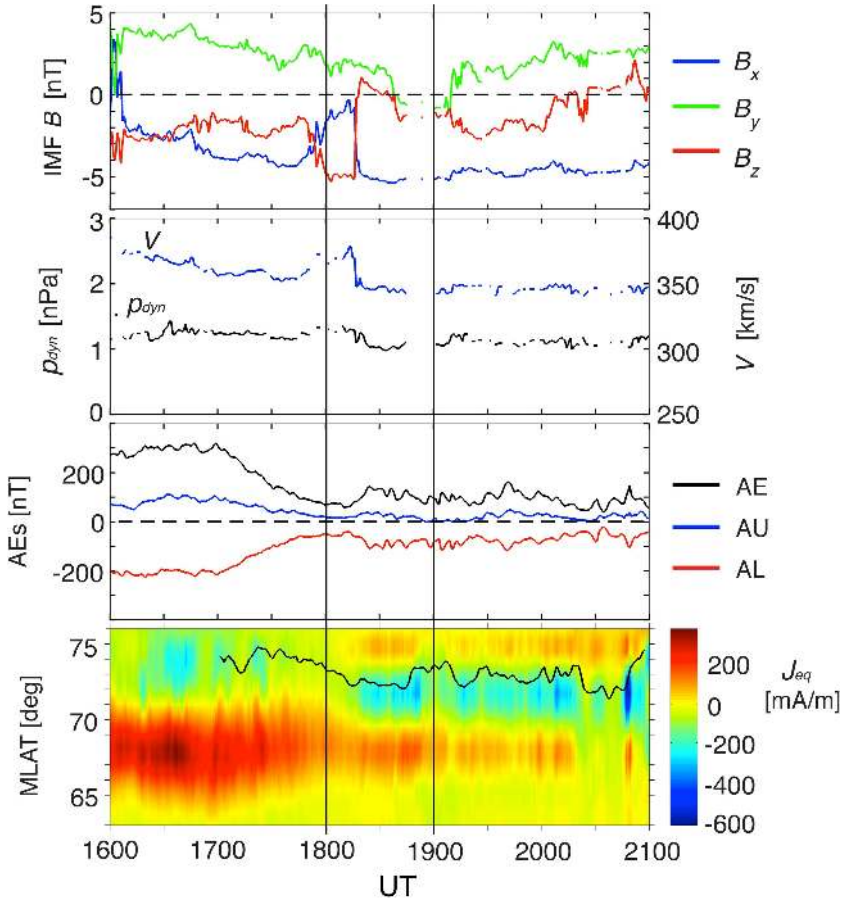

Fig. 1. Solar wind parameters by the WIND spacecraft and geomagnetic conditions on 17 October 2005. The solar wind data have been propagated to the bow shock nose ($X_{GSM} \sim 14\,R_E$). Top panel: IMF components in GSM. Second panel: Solar wind speed and dynamic pressure. Third panel: Auroral electrojet indices. Bottom panel: Equivalent east-west currents from the MIRACLE magnetometer data. Red and blue colours indicate east- and westward flowing electrojets, respectively. The polar cap boundary estimated by EISCAT is marked by a black curve. The vertical lines bound the time interval of interest.

available only for the C1 spacecraft and CODIF data were available for C3 and C4. The FGM data were available for all spacecraft. The HIA and CODIF data were provided with a spin (∼4 s) and 2-spin time resolutions, respectively. The FGM data were provided with a time resolution of one-spin.

Figure 4 presents Cluster data from the period 18:00–19:00 UT. Top two panels (a and b) show the components of the total velocities for ions measured by HIA on C1 and for protons by CODIF on C4. A running mean over three samples has been calculated for both the HIA and CODIF data. The averaging of the two data sets was needed to reduce fluctuations in the data.

Negative magnetic field B_x components (spin-resolution data, blue lines in panels c–f) show that the spacecraft were traversing the field lines of the Southern Hemisphere. In addition, plasma ion and proton β stayed over 0.5 for C1 and C4, respectively (not shown), indicating that Cluster were located in the southern inner plasma sheet (Angelopoulos et al., 1994).

According to the original definition by Angelopoulos et al. (1992, 1994), BBFs were defined to be segments of continuous ion flow speed above 100 km s^{-1}, with at least one sample >400 km s^{-1} and plasma $\beta > 0.5$. Samples >400 km s^{-1} being less than 10 min apart were considered to belong to the same BBF event, regardless of the flow speed magnitudes between these two samples. Schödel et al. (2001) introduced rapid convection events in analogy to BBFs and used a criterion for the convection electric field $E_C = [(V_x B_z)^2 + (V_y B_z)^2]^{1/2} > 2$ mV m^{-1}. Based on ion distributions of high-speed flows, Raj et al. (2002) found perpendicular flow speed >250 km s^{-1} or $\beta_{xy} > 2$ condition to be an optimal selection criterion to distinguish bulk flows from field-aligned beam events.

However, here we investigate BBFs in an event study and hence we do not use such strict quantitative criteria for BBFs as in previous statistical studies. Instead, we visually searched for perturbations in the convection velocity components measured by C1, rising above the background

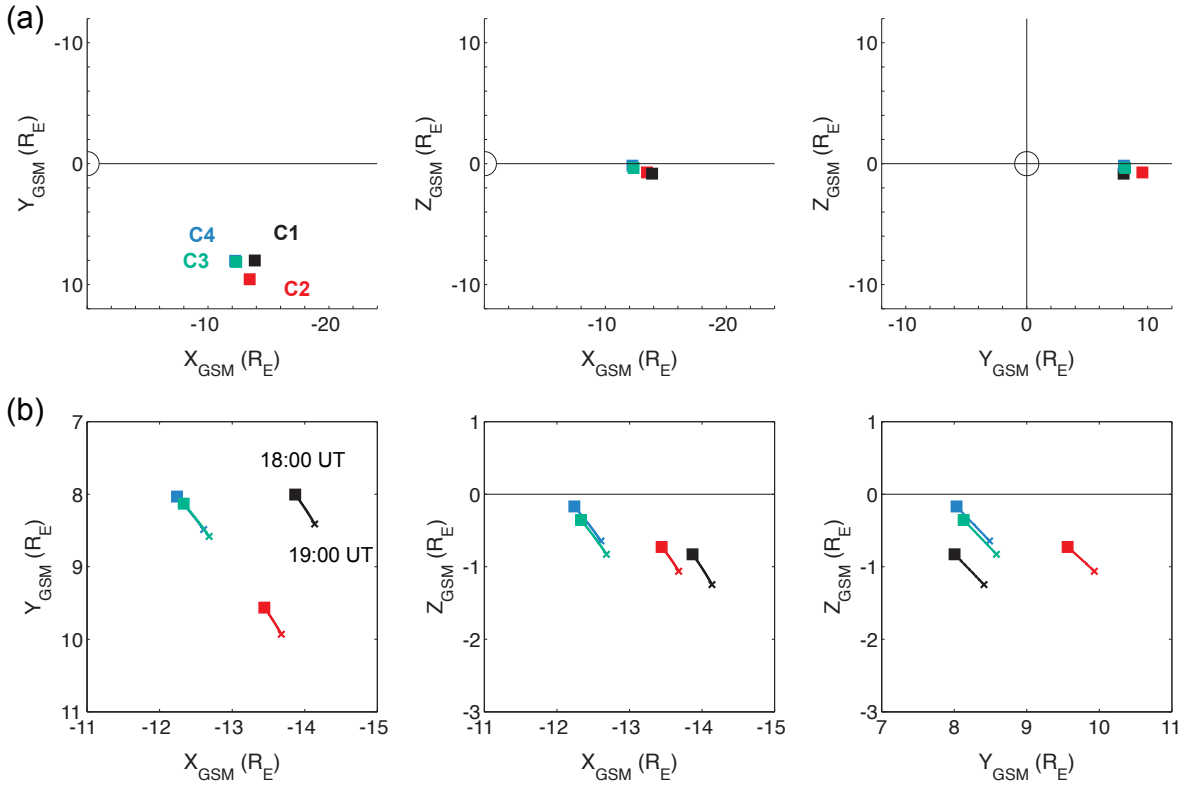

Fig. 2. (a) Cluster spacecraft positions in GSM coordinates on 17 October 2005 at 18:00 UT. **(b)** Zoomed view showing Cluster trajectories from 18:00 (square) to 19:00 UT (cross).

convection level. Consequently, three flow events could be distinguished in the velocity data of C1, including both Earth- and tailward flows, marked as 1–3 in panel (a). The flow speeds in the events peak at 100 km s^{-1}, 400 km s^{-1} and 300 km s^{-1}, respectively. Flow event 3 was seen by C4 (panel b) after a short delay compared to C1. Flow event 1 measured by the HIA sensor at C1 has such a small amplitude that it could not be distinguished from the fluctuations in the CODIF velocity data at C4, even if it would exist there. In flow event 2, C4 saw velocities just above the background level, but a clear difference to flows at C1 can be seen. The implications of these differences are discussed later.

The flow events were associated with magnetic perturbations seen also by C2 and C3, for which velocity data were not available (panels c–f). The three events are marked by grey-shaded vertical strips in Fig. 4. The time intervals were selected visually by comparing to the structures observed in the velocity and/or magnetic field data by C1. We notice that generally the perturbations in the velocity and magnetic field data were first observed by C1, then C2, C3 and C4, which is the order how satellites are located in the X_{GSM} direction, indicating that the perturbation structures were propagating Earthward (Fig. 2b). Magnetic perturbations associated with flow event 1 were not measured by C3 and C4.

However, it is beyond the scope of this paper to analyze the data in Fig. 4 in detail. In the following, we use C1 data as a guideline, since it characterizes the event well. Data from other satellites are discussed to make conclusions of the spatio-temporal extension of the events.

Figure 5 presents various parameters measured by the C1 spacecraft from CIS HIA and FGM instruments. Panel (a) shows the total ion velocity (same as in panel a in Fig. 4), whereas panel (b) shows only the component perpendicular to B, i.e. the convection velocity. The first flow event started at C1 at about 18:15 UT with a convection burst Earthwards (positive V_x) and duskwards (positive V_y) (panels a and b). The total flow turned Earthwards for a short moment (panel a) before rotating tailwards (dashed line) via the dawnward direction. During the convection burst the plasma density was slightly increased (panel g), which could be a signature of ambient plasma compression in front of an approaching plasma bubble in the BBF bubble model. Similar feature for a BBF has been reported by Snekvik et al. (2007). Indication of plasma deflection in front of Earthward-moving BBFs has been also reported by Slavin et al. (2003) and Walsh et al. (2009). The rotation of the flow tailward via dawnward direction is consistent with the expected return flow around the dawnward edge of a plasma bubble (Birn et al., 2004).

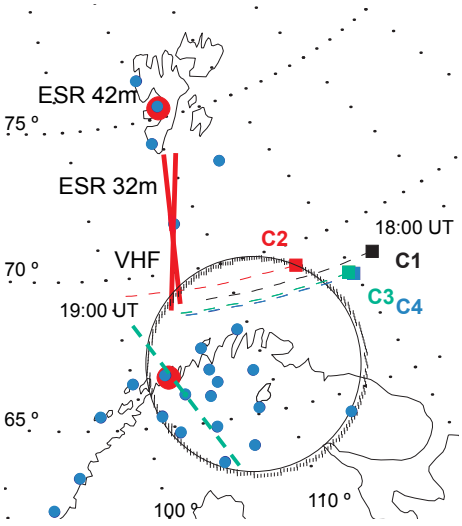

Fig. 3. Ground-based instrumentation used in this study. Red spots mark the EISCAT radar antenna locations in Tromsø (VHF, aacgm: 66.6° MLAT, 102.9° MLON) and on Svalbard (ESR 32 m and 42 m, aacgm: 75.2° MLAT, 111.9° MLON). The VHF and ESR 32 m radar beams are drawn by red lines. Blue dots mark stations of the MIRACLE magnetometer network and the black circle the field of view of the KEV ASC (aacgm: 66.3° MLAT, 109.2° MLON) mapped to an altitude of 110 km. Green dashed line centered at Kilpisjärvi (aacgm: 65.9° MLAT, 103.8° MLON) indicates the measurement range of the KIL MSP. The mapped Cluster trajectories (T96) between 18:00–19:00 UT are shown by dashed lines using the same colour-coding for the spacecraft as in Fig. 2.

At the same time when C1 observed the flow rotation tailward, the ***B*** field at C2 was significantly disturbed (Fig. 4, panel d). The positive δB_y observed by C2 in the beginning of the perturbation gives indication of that the spacecraft encountered plausibly an Earthward moving BBF from the duskside of the bubble in the bubble picture ($\delta B_y < 0$ on the duskside in the Northern Hemisphere and $\delta B_y > 0$ in the Southern Hemisphere, Sergeev et al., 1996). No disturbances were seen by the other spacecraft (panels e and f). Since at the same time C1 observed the dawnside return flow rotation as C2 measured the duskside magnetic field draping, we infer that the width of the possible BBF-like structure was about the cross-tail separation of the two spacecraft, $\sim$1.5 R_E (Fig. 2b, left panel), which is on the range of the BBF widths observed before (1–5 R_E, e.g. Nakamura et al., 2001b, and references therein). In addition, since clear signatures of a BBF proper flow were seen neither by C1 or C4, the flows inside the bubble never hit either of the satellites, but possibly the narrow BBF channel was oriented close in the GSM X direction and could be drifting slowly duskwards on the tailward side of Cluster (see the schematic illustration of the possible situation in Fig. 6a).

The second BBF flow event started at C1 at about 18:30 UT with clear signatures of the duskward side of the bubble hitting the spacecraft (Fig. 5, see also the schematic illustration of the possible situation in Fig. 6b). The Earth- and duskward convection burst (panel b) was associated with increased plasma density (panel g) and positive δB_y (panel d), the latter measured later on also by the other spacecraft (panels d–f in Fig. 4), which indicate compression and deflection of background plasma ahead the bubble with draping of the magnetic field. Generation of magnetic shear on the duskside edge of the bubble is expected to cause field-aligned current flowing to the magnetospheric shear region out of the ionosphere.

At about 18:31 UT the zonal flow turned dawnward (vertical solid line) and the following flow burst with a significant dawnward component ($V_y \sim -250\,\mathrm{km\,s^{-1}}$, panel a) was associated with a slight increase in B_z (panel d). During the latter part of the flow burst, the plasma density had a sharp decrease together with a simultaneous increase in $T_\perp$ (panel f). Since these features agree with signatures typically related to the proper flow of a BBF, like increase in B_z, plasma depletion, and increase in temperature (e.g. Ohtani et al., 2004), we interpret the flow enhancement as the proper flow of the BBF.

Typically bulk flows in the plasma sheet observed close to the neutral sheet are mostly convective and farther away from the neutral sheet they become more field-aligned (e.g. Raj et al., 2002). In this case the proper flow was dominated by a significant field-aligned component (panel c), which agrees with that Cluster was not located in the vicinity of the neutral sheet.

The flow rotation tailwards after 18:33 UT (dashed line) occurred so that V_x turned first tailwards and only after that the V_y component changed its direction from dawnward to duskward (panel a). This indicates that the tailward flow represented the BBF return flow around the dawnward edge of the bubble (Birn et al., 2004), and consequently that the C1 spacecraft exited the bubble across the dawnside boundary. From these observations we infer that the BBF channel was drifting duskward across the Cluster location. According to the bubble model, at the dawnward edge of a bubble a downward field-aligned current should flow into the ionosphere. This dawnside field-aligned current has been recently observed in the magnetotail by Snekvik et al. (2007).

As becomes evident later, the third BBF event is divided into two parts, 3a and 3b (Fig. 5). The first part 3a, seen by C1 after 18:40 UT, was preceded by a short convection pulse Earth- and duskwards. This pulse was probably related to a transient disturbance that passed Cluster farther on the dawn side since it is seen as an almost simultaneous compression in the magnetic field by all the spacecraft, caused by perturbations in the B_x and B_y components (Fig. 4).

The pre-pulse was followed immediately by another stronger convection pulse 3a of the BBF (Fig. 5, panel b). The Earth- and duskward convection burst was associated with an increase in plasma density (panel g), which suggests again plasma compression and deflection in front of a bubble,

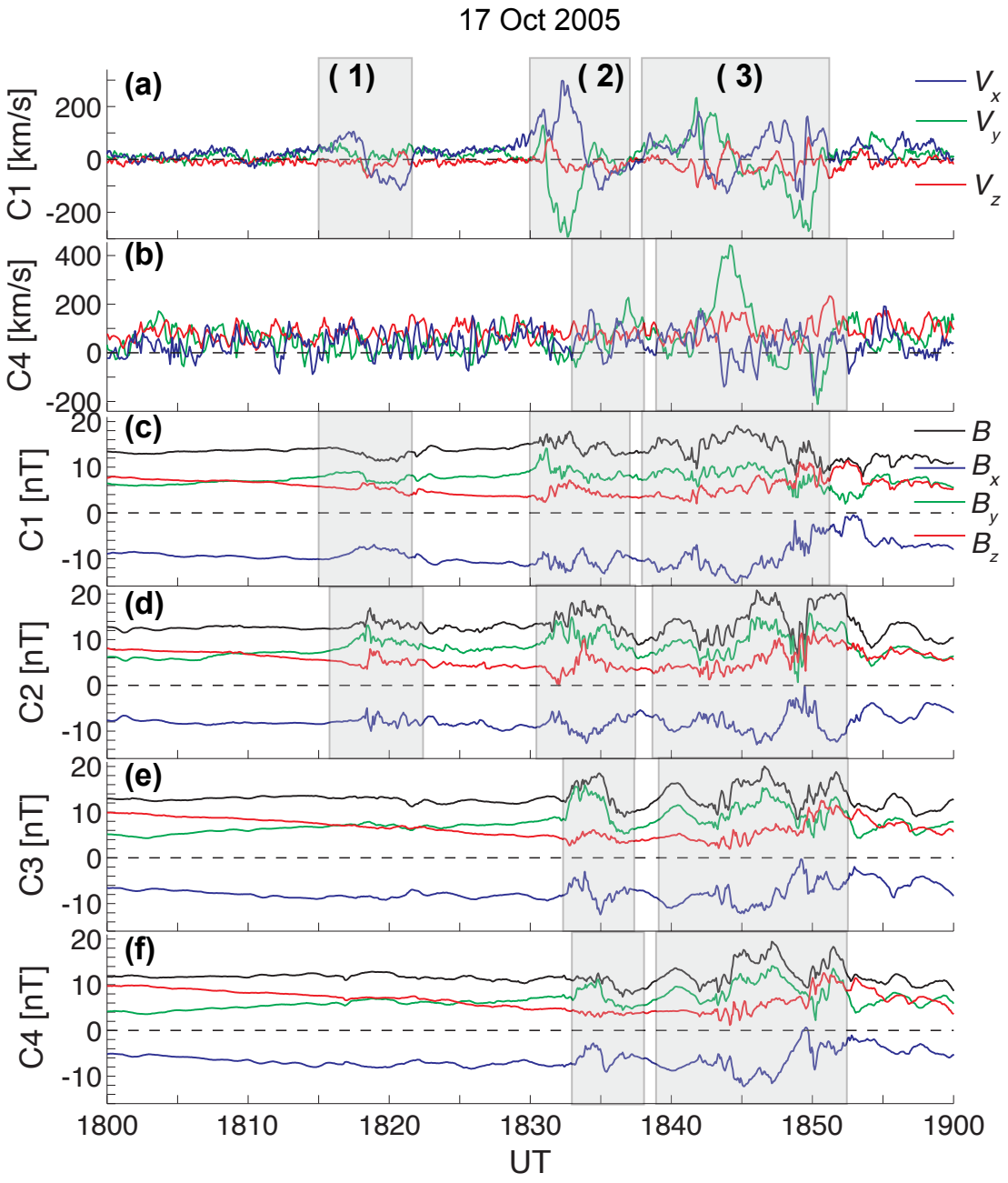

Fig. 4. Cluster data on 17 October 2005. **(a)** C1 CIS HIA velocity components in GSM. **(b)** C4 CIS CODIF proton velocity components in GSM. **(c)**–**(f)** Spin resolution magnetic field components by FGM in GSM. The vertical grey-shaded strips indicate the flow events under study.

located on the dawnside of the satellites (see the schematic illustration of the possible situation for this event in Fig. 6c).

After that, the total plasma flow rotated tailward while maintaining the duskward component (panel a), which indicates a return flow on the duskside of the bubble. In this case, no proper flows were observed in Cluster, so there was no indication of a duskward drift of the flow channel as in previous events of this study. The flow return was associated with a clear decrease in plasma density after 18:41 UT (panel g) with simultaneously increased $\boldsymbol{B}$ field (cf. magnetic pressure in panel e), which implies that the duskside return flow consists of depleted but compressed flux tubes.

The vortical flow pattern was associated with bipolar variations in the magnetic field seen also by other spacecraft (Fig. 4, panels d–f). The C4 satellite observed a strikingly similar flow pattern with a significant duskward component

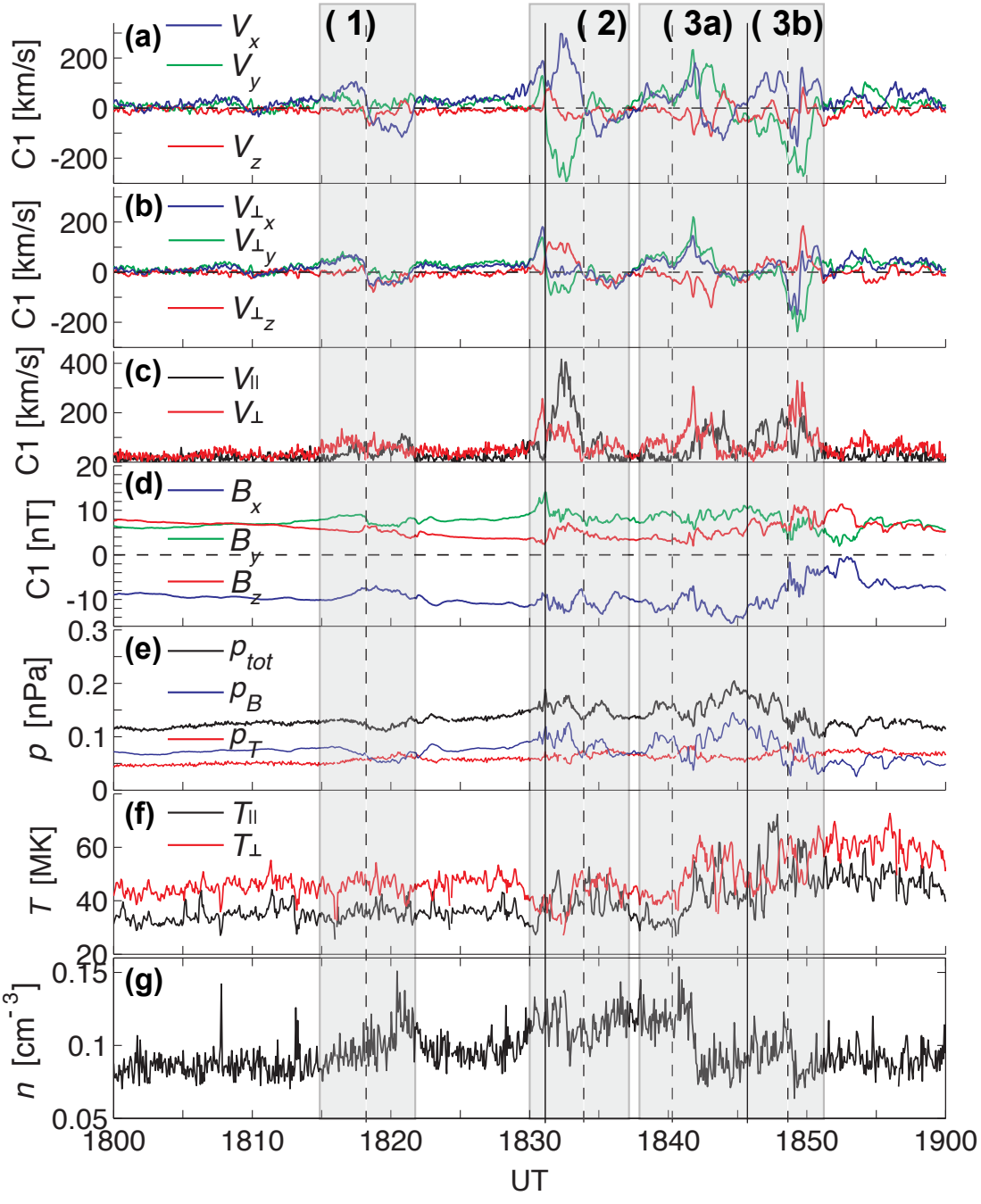

Fig. 5. Cluster C1 data. **(a)** CIS HIA total velocity in GSM. **(b)** CIS HIA velocity perpendicular to the magnetic field. **(c)** Magnitudes of the parallel and perpendicular velocity. **(d)** Magnetic field. **(e)** Total pressure (black), thermal pressure $p_T = nk_B(T_{||} + 2T_\perp)/3$ (red) and magnetic pressure $p_B = B^2/(2\mu_0)$ (blue). **(f)** Parallel ($T_{||}$) and perpendicular ($T_\perp$) temperatures used in thermal pressure calculation. **(g)** Ion density. The vertical grey-shaded strips indicate the BBF events under study. Solid vertical lines mark the start of the proper flow of a BBF at C1. Dashed vertical lines mark major changes in the flow, see details in the text.

during the return flow ($V_y \sim 400\,\mathrm{km\,s^{-1}}$, Fig. 4, panel b). The return flow at C4 was also associated with decreased plasma density (not shown).

The flow pattern after 18:45 UT, labelled as 3b, evolved as an Earth- and dawnward velocity burst with two-hump substructure (Fig. 5, panel a). The burst showed again small enhancements in B_z (panel d) and increases in temperatures (panel f), hence we interpret the burst as the proper flow of BBF event 3b. As in event 2, the proper flows were dominated by the field-aligned velocity component (panel c).

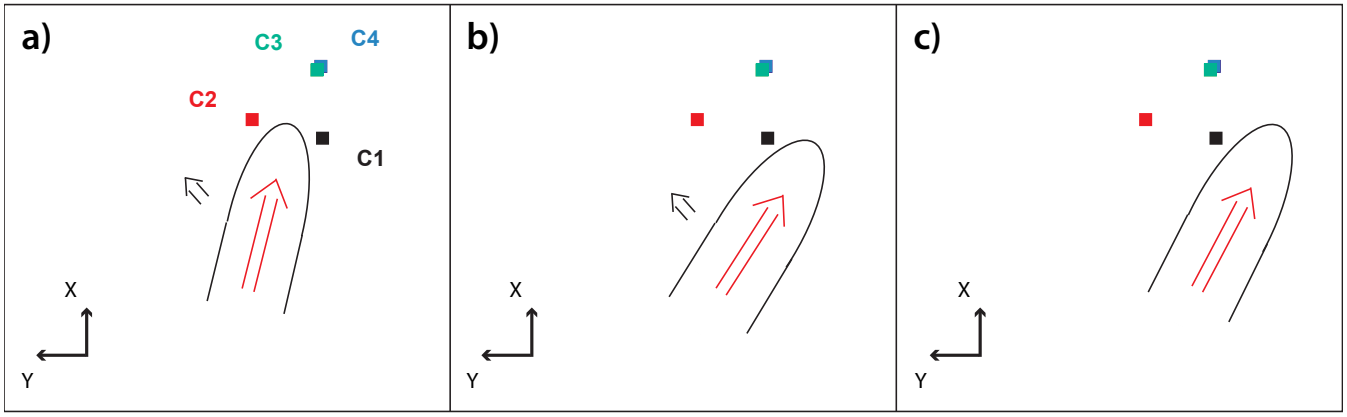

Fig. 6. Schematic illustrations for possible configurations of the BBF flow events in the GSM XY plane. Red and black arrows indicate the direction of the BBF proper flow and azimuthal drift direction of the flow channel, respectively. Frame **(a)** Event 1 at about 18:18 UT when C2 observes the magnetic signatures on the duskside and C1 sees the dawnward return flow of the BBF. Frame **(b)** Event 2 at about 18:30 UT when C1 encounters the BBF. Frame **(c)** Event 3a at about 18:41 UT when C1 encounters the BBF. Note, that in this case no significant duskward motion of the flow channel was observed.

After 18:48 UT the flows at C1 turned tailward (dashed line) and a convection burst lasting about 1.5 min took place (panel b). At the same time, the magnetic field data showed increase in B_x towards zero at the positions of the C2, C3, and C4 satellites, which suggests that the neutral sheet was locally flapping southward (Fig. 4, panels d–f). Earth- and duskward convecting neutral sheet flux tubes were observed by C4 (Fig. 4, panel b, total velocity in this case was dominated by convection, not shown) that probably displaced and pushed the ambient flux tubes tail- and dawnwards, as seen by C1. Flapping was plausibly caused by a disturbance passing the satellites on the dawnward side interfering with event 3b.

During the tailward flow burst at C1 after 18:48 UT, the magnitude of $\boldsymbol{B}$ field increased (B_x decreased, B_z increased, Fig. 5, panel d) and plasma density decreased (panel g). Satellites C2, C3 and C4 observed similar signatures of flux tube compression (Fig. 4d–f) and C4 measured also plasma depletion (data not shown), giving support for the scenario of the duskside return flow being composed of compressed but depleted flux tubes.

In the next sections we aim at building a comprehensive picture about the BBF events described above by combining the Cluster and EISCAT measurements with additional ground-based data provided by the MIRACLE network and a meridian-scanning photometer.

2.3 Ionospheric data

Figure 7 shows Cluster C1 and C4 ion velocities from the plasma sheet and EISCAT VHF radar measurements from the conjugate ionosphere between 18:00–19:00 UT.

Panels (a) and (b) contain the same velocity data for C1 and C4 spacecraft as panels (a) and (b) in Fig. 4, respectively. Panels (c)–(f) show the line-of-sight (l-o-s) ion velocity V_i, electron temperature T_e, electron density N_e and ion temperature T_i measurements by the VHF radar. The VHF radar was measuring using the tau8 modulation and the data have been integrated to 1-min time resolution. The data shown are from the altitude range of 130–545 km, which corresponds to a latitude range of 68.8–74.3° MLAT. The height resolution changed from 10 to 33 km, as the latitudinal resolution changed from ∼0.15 to 0.3° MLAT in the poleward direction.

The black continuous line between 72° and 74° MLAT in panels (c), (d) and (f) is the estimate for the polar cap boundary (PCB). A running mean over 3 min has been calculated from the 1-min PCB data. The PCB was extracted from the VHF and ESR 42 m radar T_e measurements by using the ΔT_e-method by Aikio et al. (2006) (see also Hubert et al., 2010), in which the ESR 42 m radar provides the reference T_e altitude profile from the polar cap. In the ESR radar the tau0 modulation was used. The ESR 42 m data used were measured from the altitude range of 98–714 km with the height resolution changing from the lowest E-region values of 4 km up to 36 km high in the F-region. The data were first integrated to 1-min time resolution and then averaged over 1-h in the method (see Aikio et al., 2006, for details). From panel (d) one can see that T_e observed by the VHF radar is elevated on the closed field line region by particle precipitation and T_e is lower within the polar cap.

Figure 7 shows that several equatorward moving structures in the four plasma parameters were seen by the VHF radar (panels c–f). The times of the appearance of the structures at the VHF radar suggest direct connection to the corresponding BBFs observed by Cluster in the plasma sheet (panels a–b).

In the ionosphere, BBF-associated auroral streamers are expected to be seen in the radar as locally elevated F-region

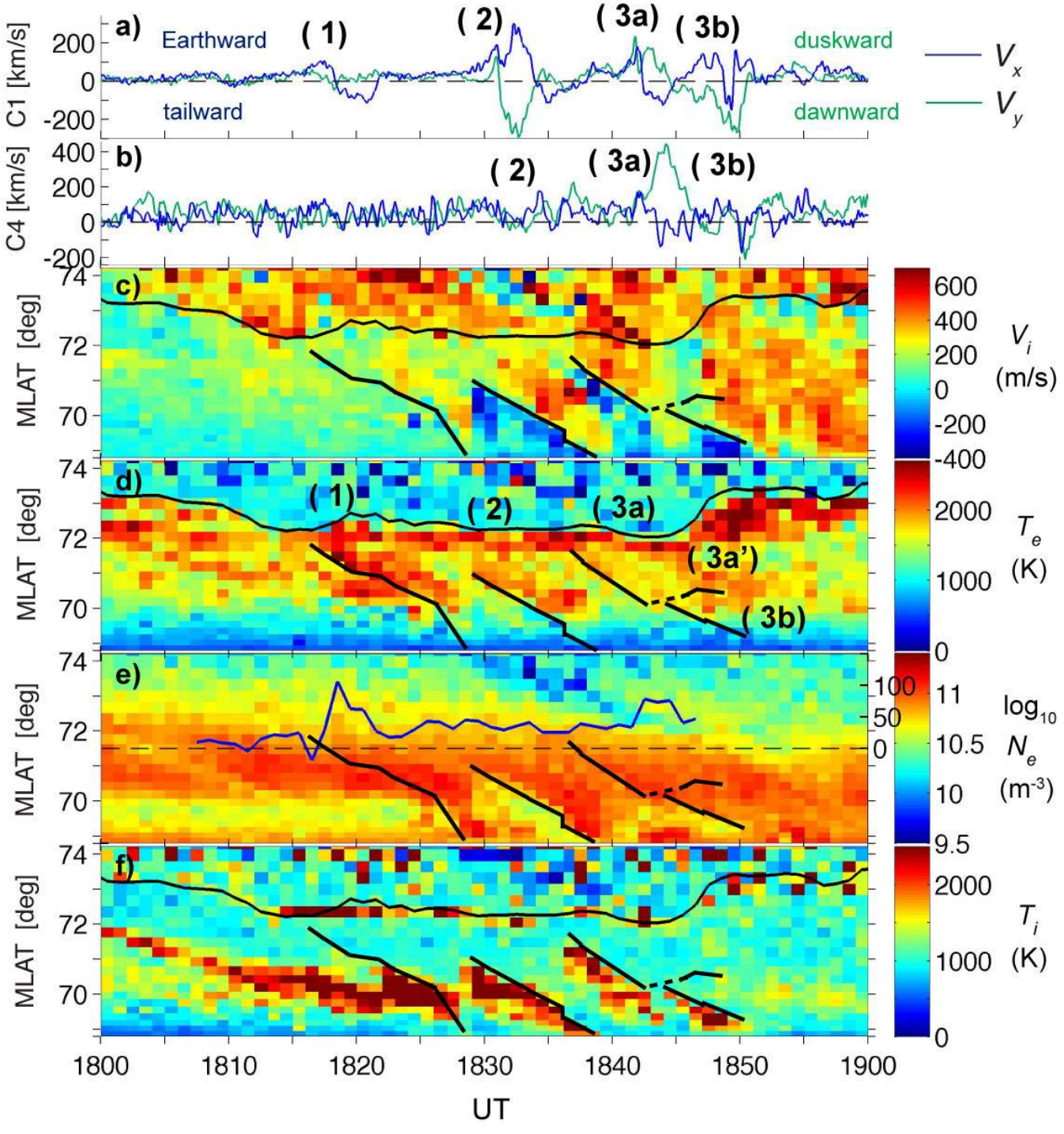

Fig. 7. Cluster and EISCAT VHF data from the time interval 18:00–19:00 UT. **(a)** and **(b)** The same as in panels (a) and (b) in Fig. 4, but without V_z component. **(c)–(f)** Line-of-sight ion velocity (V_i, positive towards the radar), electron temperature (T_e), electron density (N_e), and ion temperature (T_i). Black continuous line in panels **(c)**, **(d)** and **(f)** marks the polar cap boundary. Blue line in panel **(e)** is the reconnection electric field estimate. Note the separate scale ($mV\,m^{-1}$) on the right for the E_r. Velocity shears associated with the auroral streamers are marked by black thick equatorward descending lines in panels **(c)–(f)**. The dashed portion marks the appearance of streamer 3b equatorward of 3a.

electron temperature within the auroral form due to collisional heating by precipitating particles, and as enhancements in the E-region and lower F-region electron densities (N_e) due to precipitation itself. This is exactly what is seen in panel d: narrow enhanced T_e bands drift equatorward and continue to lower latitudes. Lower latitudes correspond to lower altitudes in the radar data and there streamers are seen as enhanced N_e (panel e). The streamers detaching from the polar cap boundary are marked in panel (d) by the same numbering as the related BBFs in panels (a) and (b).

A sharp plasma velocity shear appeared at the equatorward edge of streamers 2, 3a and 3b in the l-o-s velocity measured by the VHF radar and is marked by a black thick line to panel (c) (visual inspection), as well as to the other panels d–f. The same line is marked also for streamer 1, but in that case no clear flow shear was visible in the VHF data and the location was deduced from the T_e data (panel d). The dashed thick line marks the appearance of the streamer 3b. Details of event 3 are given in Sect. 2.3.2.

The ionospheric plasma flow within the streamer and on the poleward side had an equatorward component. The plasma flow with a poleward component on the equatorward side of the streamer was associated with low electron density (panel e) and enhanced ion temperature (panel f). The latter indicates frictional heating between ions and neutrals. Since we do not have a reliable estimate of the electric field within the region of increased T_i, we do not know the magnitude nor the direction of electric field. However, the situation may bear resemblance to evening sector auroral arcs, where an enhanced northward electric field is often found on the equatorward side of the arc (Aikio et al., 1993).

Next, we will interpret Fig. 7 together with optical all-sky camera measurements of auroral streamers and other ground-based data (Figs. 8 and 10). Since the auroral streamer associated with BBF event 1 hardly penetrated the poleward boundary of the field-of-view of the Kevo all-sky camera, we will not study it here in detail.

2.3.1 BBF event 2

Figure 8 presents a set of frames of conjugate ground-based data between 18:29:00–18:38:00 UT during BBF flow event 2. The frames have been oriented to show the data as it would look like in the polar MLT-MLAT coordinate system. The local time sector covered by the ground-based data is roughly 20:50–22:20 MLT.

The circle shows the f-o-v of the Kevo all-sky camera (KEV ASC). The auroral emission intensities were recorded every 20 s through the 557-nm filter using a one-second exposure time. The emissions have been mapped to an altitude of 110 km, which is approximately the lower border for 5–10 keV precipitating electrons. The intensities are given in Analog-to-Digital Units (ADUs), which for the used camera vary in the range 0–255 (8-bit resolution). Note that mapping of the ASC data is not accurate on the edges of the f-o-v.

The white dashed lines across the f-o-v of the KEV ASC from frame c onwards indicate the region of the 486 nm (Hβ) proton aurora. The Hβ oval was inferred from the KIL meridian-scanning photometer (MSP) observations at the westward edge of the KEV ASC (Fig. 3) by assuming emission altitude of 110 km, and then extended as an approximation along the constant aacgm latitudes over the f-o-v of the KEV ASC. Hβ emissions result from energetic proton precipitation with typical energies of 1–30 keV. The equatorward boundary of the oval can be taken as a proxy for the isotropic boundary for these protons which means that equatorward of the boundary the field lines are dipolar enough for the ions to move adiabatically with empty loss cone (e.g. Kauristie et al., 2003, and references therein). The location of the proton oval stayed stable in the KIL MSP during the period of the BBF-streamer events.

The auroral streamer activated in the KEV ASC data already at ~18:28 UT (not shown) and at 18:29:00 UT it had intruded across the poleward edge of the KEV ASC f-o-v (Figs. 8a–b). After braking of the streamer on the northeast edge of the ASC (Fig. 8c), the most intense emissions faded and the streamer started to drift westward along the poleward boundary of the proton oval (Figs. 8d–f). The auroral form also turned more north-south aligned. At around 18:36 UT a transient (~1 min) activation took place (Fig. 8e) before the streamer dissolved in patches (Fig. 8f).

The two adjacent poleward aligned colour bars northwest of the ASC f-o-v indicate electron temperature (west) and ion l-o-s velocity (east) measurements by the VHF radar. The same colour scale and time resolution as in panels (d) and (c) of Fig. 7 are used for T_e and V_i, respectively. The five lowest (equatorwardmost) gates in the T_e bar have been replaced by N_e data in all frames in order to be able to follow the streamer as far southward as possible in the upper E-region.

The EISCAT VHF radar measured the streamer northwest of the KEV ASC during 18:29–18:39 UT as the enhanced electron temperature band in the F-region data (Fig. 7d, marked on the T_e bar in Fig. 8 by a red ellipse). In the end of the period, the streamer and its remnants were visible also in the upper E-region N_e data (Fig. 7e and Figs. 8e–f), possibly until 18:40 UT, which gives an estimate for the duration of the streamer to be about 10 min. The north-south cross-width of streamer 3b along the VHF radar beam estimated from the T_e data was ~0.7° MLAT.

The ion velocity (V_i) data shows flows toward the radar within and on the poleward side of the T_e enhancement, and away from the radar on the equatorward side. The location of the flow shear is marked by a black line in Fig. 8 and it is extended as a dashed line toward the f-o-v of the ASC. We interpret that the 2-D convection pattern was southeastward on the poleward side and northwestward on the equatorward side of the velocity shear, so that the flow lines were mainly aligned along the streamer direction.

The interpretation is based on the previous observations that a streamer corresponds to the upward field-aligned

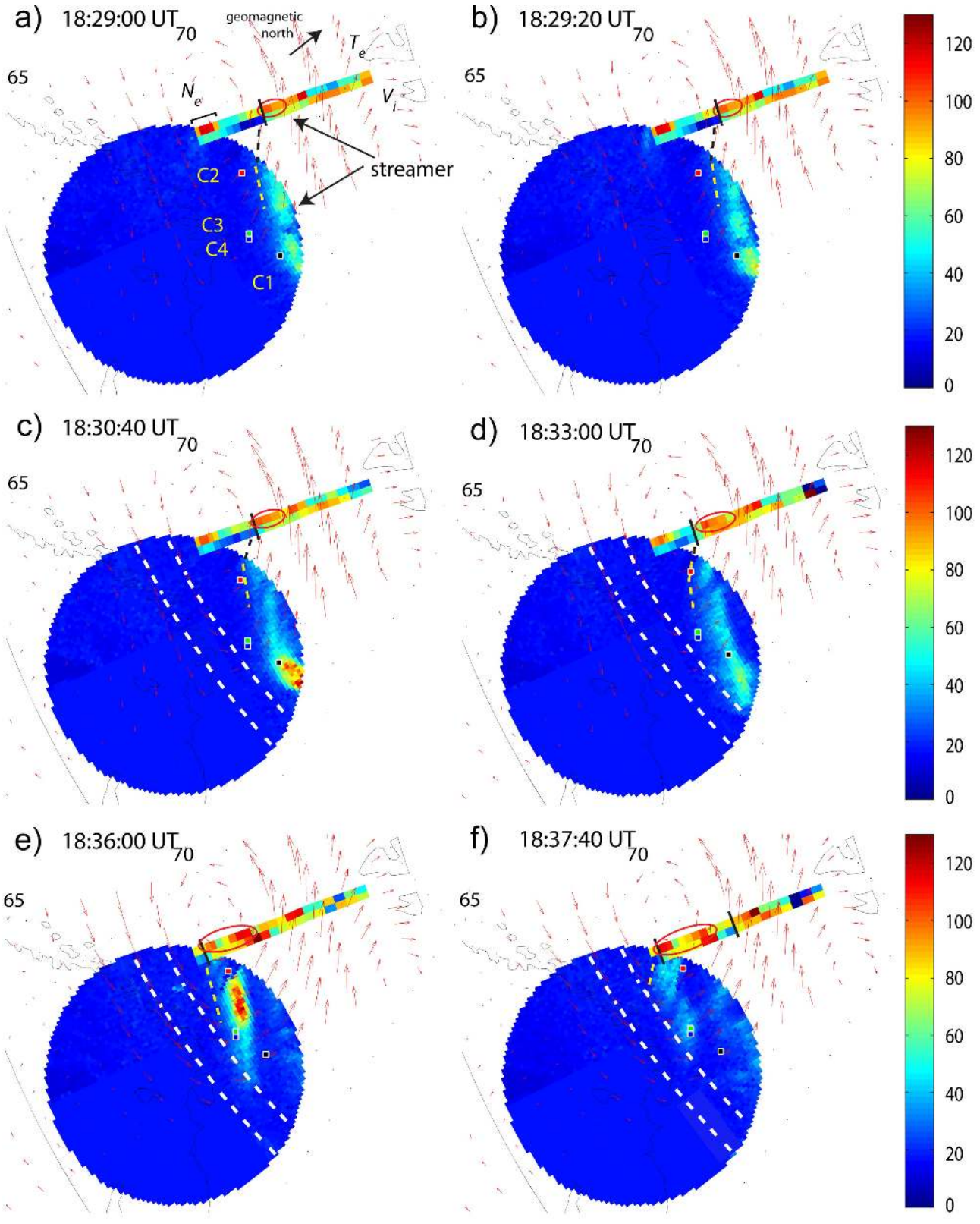

Fig. 8. A set of frames presenting the conjugate ground-based data during BBF flow event 2. The circle shows the KEV ASC data and the red arrows are the equivalent current vectors. The white dashed lines indicate the proton oval during the event. Coloured bars along the VHF radar beam are T_e (replaced by N_e at the nearest range gates), and V_i. See details in the text.

current flowing near the duskside edge of the BBF channel (e.g. Amm et al., 1999; Sergeev et al., 2000; Nakamura et al., 2001b). This interpretation is also supported by the 2-D convection vectors calculated from the combined VHF and ESR 32 m data closer to the PCB (data not shown, see details of the calculation in Discussion in connection with E_r estimation). Unfortunately, the signal-to-noise ratios for the farther gates of the ESR 32 m radar were too poor for reliable 2-D velocity vector extraction at the streamer latitudes. Hence, the plausible northwestward plasma flow on the equatorward side of the streamer was associated with low electron density and enhanced ion temperature, as discussed in the previous section.

Red arrows in Fig. 8 represent the 2-D ionospheric equivalent Hall current vectors in arbitrary units derived from the MIRACLE magnetometer data using the 2-D SECS method by Amm (1997) and Amm and Viljanen (1999). The colour squares mark the Cluster footpoints. Again, the same colour coding for the spacecraft has been used as in previous figures.

The equivalent current pattern showed northwestward directed current with counter-clockwise and clockwise vortices at its southwestward and northeastward sides, respectively (Fig. 8). This kind of an equivalent current pattern has been established to represent the ionospheric current signature of a BBF (Juusola et al., 2009, and references therein). By assuming uniform conductances one can associate the vortices with field-aligned currents, the upward field-aligned current flowing at the southwestward flank and the downward field-aligned current at the northeastward flank of the current channel. In this case, the streamer was located in the region corresponding to the upward field-aligned current. The pattern preserved its overall form during the whole lifetime of the streamer. A slight rotation of the northwestward current vectors more north-south aligned, however, can be seen in association with the turning of the streamer during its westward motion.

By mapping the Cluster positions along the field lines into the ionosphere, the plasma flows of the BBFs measured by Cluster can be compared with the ion velocities observed by EISCAT. However, it is good to keep in mind that there are always some uncertainties present in mapping since it is done by using models.

In order to investigate the flows, we mapped the Cluster positions into the ionosphere using T96 magnetosphere model. We tried slightly different solar wind input values, which were prevailing during the event and ended up in using the average values from 16:10–17:50 UT (preceding the first IMF rotation, Fig. 1). When the solar wind data from the period of increased southward IMF B_z was applied (18:00–18:16 UT, IMF $B_z \sim -5$ nT), the footpoints of Cluster moved about 0.6° MLAT equatorwards. When the mean values from the time interval of northward IMF (18:18–18:36 UT, IMF $B_z \sim 0.5$ nT) were used as input, the effect was to move the footpoints about 0.4° MLAT polewards in respect to the locations obtained by using the average IMF values. In longitude, the effect in both cases was negligible.

Besides the uncertainties in the model itself, the magnetic field reconfiguration associated with a BBF may alter the field topology in a such a way that the deviations from the model get larger. Another point is that there is always some delay expected between ionospheric signatures of magnetospheric processes due to Alfvén propagation time. However, in the following no delay has been applied to data.

At the time when Cluster C1 saw the first signatures of the approaching BBF, including the duskward deflection of flow after 18:30 UT (Fig. 7a), the spacecraft mapped on the equatorward side of the streamer close to the equatorward intruding tip of the streamer (Fig. 8b–c). At the same time, the VHF radar measured the poleward component of the flow indicating plausible northwestward flow on the equatorward side of the streamer. This suggests that the poleward flow equatorward of the streamer represents the ionospheric counterpart of the duskside tailward return flow of a bubble in the magnetosphere.

As C1 entered the flow channel from the duskside and measured the proper flow of the BBF $\sim$ 18:31–18:34 UT (Fig. 7a), the streamer was already drifting westward and the spacecraft mapped within the streamer (Fig. 8d), and a bit later on the poleward edge of it. Now the equatorward (plausibly southeastward) plasma flows measured by the VHF radar within the streamer and poleward of it are consistent with the expected ionospheric counterpart flows of the Earth- and dawnward proper flow observed by C1. The north-south cross-width of the ionospheric equatorward plasma flow channel by the VHF radar was about 1.2° MLAT.

Further evidence for the poleward flow to represent the duskside return flow at the VHF radar comes from the other Cluster spacecraft. As the streamer drifted slightly equatorward towards the footpoints of the other spacecraft during its westward motion (Fig. 8d), Cluster measured magnetic signatures of the duskward edge of the bubble ($\delta B_y > 0$) arriving first at C2 after 18:31 UT, before reaching the C3 and C4 spacecraft (Fig. 7d–f in Fig. 4). A sketch of the possible situation is presented in Fig. 9.

After 18:34 UT C1 exited the bubble and the return flow on the dawnward side was observed (Fig. 7a). The streamer had turned more north-south aligned and the footpoint of C1 was located on the poleward side, and later well poleward of the streamer, as seen in Fig. 8e. At the same time the VHF radar measured the ionospheric equatorward flow within and poleward of the streamer, and the poleward return flow on the equatorward side of the streamer. According to our interpretation, the VHF radar saw the ionospheric proper flow and the duskside return flow of BBF event 2. Poleward of these features, a region of poleward flow was seen by VHF. We interpret that it is the return flow of BBF event 3a, but it could be argued that the equatorward part of the poleward flow would be the dawnward return flow of BBF event 2, measured by C1 in the tail.

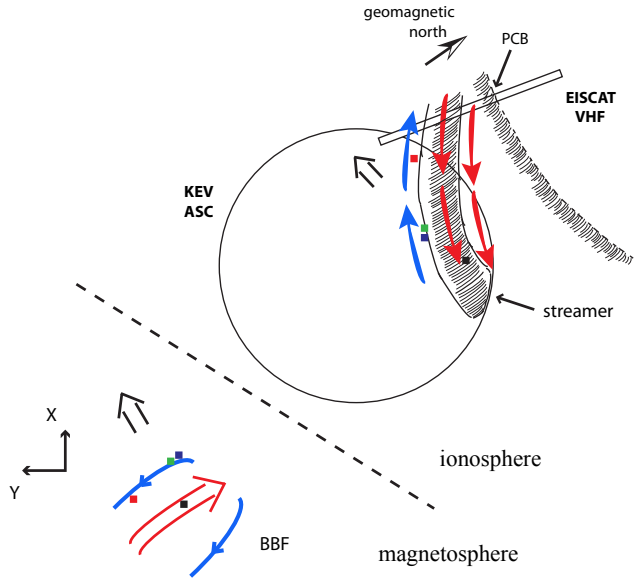

Fig. 9. Schematic illustration of the situation in the ionosphere and possible configuration of the BBF in the tail close to the XY_{GSM} plane at ∼18:31–18:34 UT when C1 sees the BBF 2 proper flow (see also Fig. 8d). Red arrows indicate the BBF proper flow and blue arrows the return flows. Wide black open arrows indicate the drift direction of the flow pattern.

After 18:34 UT C4 was located on the other side of the streamer as C1 (Fig. 8e). The velocity pattern at C4 (Fig. 7a) shows signatures of duskward deflection followed by dusk-side return flow. This is consistent with the magnetic signatures observed by the spacecraft already mentioned above and confirms the existence of the duskside return flow at the VHF radar. Figs. 8c–f show that the streamer braked and then drifted westward along the poleward boundary of the proton oval, which is consistent with the observations by Kauristie et al. (2003). In this case, the streamer tip stayed a rather long time in the vicinity of the proton oval, which is related to rather long-lived positive δB_y perturbation at C3 and C4 (panels e and f in Fig. 4). While drifting westward plausibly with the background convection, the streamer dissolved into patches starting from the most equatorward tip, which could indicate that the fast flow decayed starting from the Earthward edge.

In this case, the streamer preserved its straight orientation without diverting duskward and forming a dusk-opened U-shaped loop, as was seen by Kauristie et al. Presumably the BBF in our case was too weak to be able to intrude deep enough into the inner magnetosphere to cause flow diversion around the more dipolar field lines, as was suggested by Kauristie et al. in their case.

2.3.2 BBF event 3

The previous streamer was soon followed by an appearance of a faint streamer from 18:39 UT onwards, which was probably associated with the increase in Earth- and duskward convection seen by C1 before 18:40 UT (e.g. Fig. 7a). The feature was seen by the VHF radar in T_e enhancement detaching from the polar cap boundary already after 18:38 UT (Fig. 7d). This auroral burst was associated with an appearance of the sharp velocity shear at the equatorward edge of the streamer (Fig. 7c), having low N_e (Fig. 7e) and enhanced T_i (Fig. 7f) in the poleward plasma flow region.

Figure 10 presents a similar set of frames for BBF event 3 as was shown for the previous event in Fig. 8. Now the frames are situated approximately in the local time sector 21:10–22:30 MLT.

Streamer 3a activated from the west after 18:41 UT (Fig. 10a) and developed into an intense arc. While extending equatorward, the southern tip bent towards the poleward boundary of the proton oval (Fig. 10b). During the following westward drift of the most intense aurora, the tip of the streamer penetrated into the proton oval all the way to the equatorward edge of the oval (Fig. 10c).

All four plasma parameters showed slight equatorward migration in the VHF data (Figs. 7c–f). The enhanced T_e band, however, was not clearly visible due to the most intense precipitation concentrating on the eastward side of VHF, as seen by the KEV ASC (Figs. 10a–c). The north-south cross-width of the streamer along the radar beam estimated from the VHF T_e data was ∼0.8° MLAT.

During this period first C1 and later also C4 observed the BBF duskside deflection followed by the duskside return flow (Figs. 7a and b). The mapping of the spacecraft equatorward of the streamer is again consistent with the situation that the poleward ionospheric flow seen by the VHF radar represents the ionospheric counterpart of the duskside return flow in the bubble picture. A sketch of the situation in this case is presented in Fig. 11.

After 18:45 UT another streamer 3b intruded on the equatorward side of the fading and westward retreating streamer 3a (Fig. 10d) pushing it slightly poleward. The new streamer was seen first by VHF west of the KEV ASC probably already right after 18:45 UT (equatorward red circle in Fig. 10c). After 18:47 UT the more equatorward streamer 3b was clearly visible in the VHF T_e data (Fig. 7d, Fig. 10d). The north-south cross-width of the streamer 3b along the VHF radar beam was estimated from the VHF T_e data to be ∼0.7° MLAT. The intrusion of streamer 3b was also associated with the appearance of the sharp velocity shear at the equatorward edge of the streamer (Fig. 7c). Ionospheric plasma flow within the two streamers had an equatorward component.

In event 3a, the plasma flow had an equatorward component all the way from the velocity shear up to the polar cap boundary. However, the absolute upper limit for the width

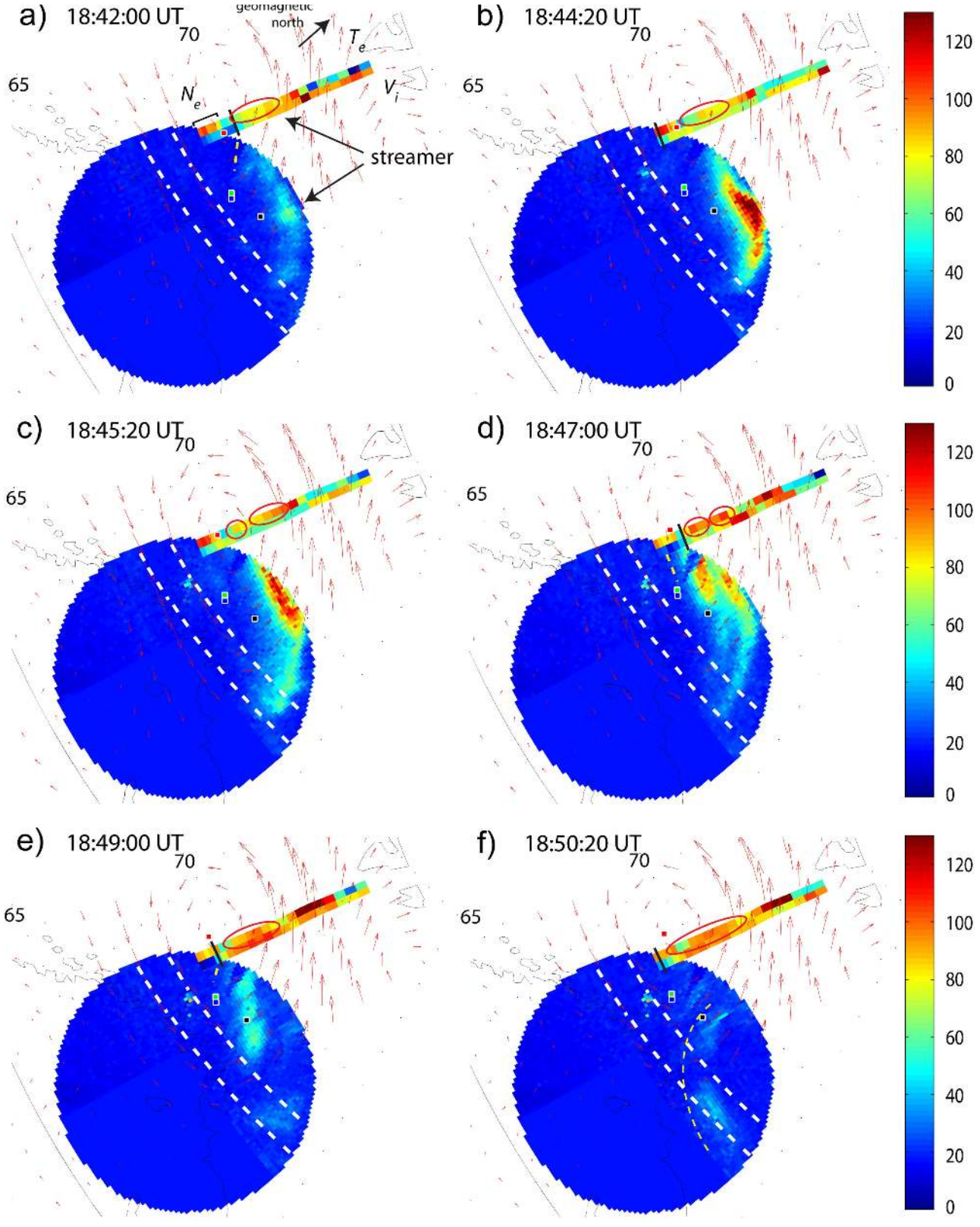

Fig. 10. Same as Fig. 8, but for BBF flow event 3. See the other details in the text.

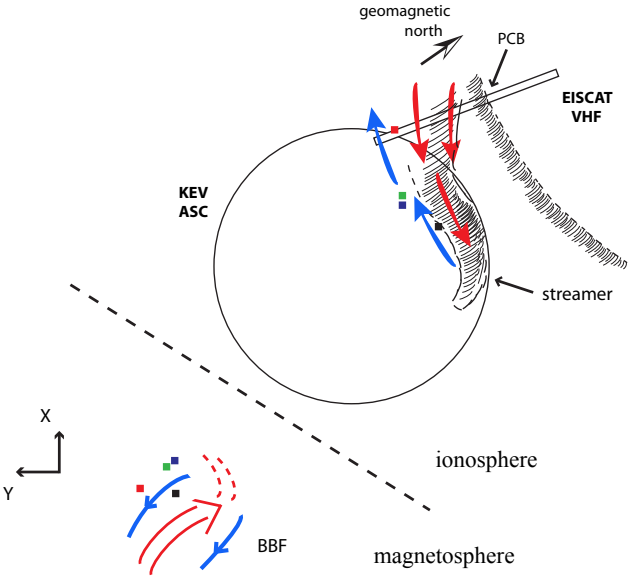

Fig. 11. Same as Fig. 9 for ∼18:42–18:45 UT when C1 sees the duskside return flow of BBF 3a (see also Fig. 10b).

of the flow channel could be obtained from the time interval 18:42–18:43 UT when the separation of the velocity shear and the PCB was greatest before appearance of streamer 3b. The maximum north-south cross-width for the ionospheric equatorward plasma flow channel during streamer 3a was about 2° MLAT. After appearance of streamer 3b the ionospheric flow channel widths could not be estimated.

The time period 18:45–18:48 UT, when streamer 3a was pushed polewards by streamer 3b on its equatorward side, is indicated by 3a′ in Fig. 7. The line 3a′ is drawn at the southern edge of the streamer 3a location. At the end of this time period, the streamers merged and the remnant auroral form turned more north-south aligned while drifting westward along the poleward boundary of the proton oval (Fig. 10e). During the merging, the tip of streamer 3a inside the proton oval separated from the remnant and developed to a northeast opened curve-like arc, which drifted westward over the f-o-v of the KEV ASC (Fig. 10f). The life-times of streamers 3a (including first signatures after 18:38 UT onwards) and 3b (including merged 3a′-3b form in the late phase) observed by VHF were about 11 min and 7 min, respectively.

During the time of the intrusion of streamer 3b, Cluster C1 mapped roughly on the location where the ionospheric plasma flow was equatorward (southeastward) (Fig. 10d). At the same time the spacecraft observed the proper flow of the BBF event 3b (Fig. 7a), which suggests that also in this case EISCAT and Cluster caught the same proper flow of the BBF.

Figure 10a–d shows that the tip of streamer 3a turned duskward forming a hook-like structure on the equatorward end of the most intense emissions. This is a similar feature that was seen by Kauristie et al. (2003) and it suggests that the flows at the Earthward end of the BBF flow channel were diverted towards dusk in the inner magnetosphere. During the westward motion of the merged streamer started to fade from Earthward end, which again indicates that the flows started to decay starting from the Earthward.

The westward moving curved larger-scale auroral form (Fig. 10f) was probably related to the local reconfiguration of the field lines and convection in the vicinity of Cluster due to the flapping of the neutral sheet by a transient larger-scale disturbance, as was discussed in Sect. 2.2. The north-south alignment of the poleward part of this auroral form supports the interpretation that the velocity pattern observed by C1, and later also by C4, after the BBF event 3b proper flow from 18:48 UT onwards (Figs. 7a–b) was associated with this auroral feature.

During the whole period, the 2-D equivalent currents showed a similar pattern as was seen during event 2, and the two streamers were formed in the southwestward flank of the northwestward current in the region corresponding to the upward field-aligned current. Again, a slight rotation of the current vectors more north-south aligned occurred during the turning of the merged streamer remnant during its westward motion.

3 Discussion

The EISCAT VHF radar provides high-resolution measurements of BBF-related flows in the ionosphere. Comparison with the Cluster data shows remarkable correspondence between the flows in the plasma sheet and in the conjugate ionosphere. The flow patterns both in the magnetosphere and in the ionosphere are consistent with the bubble picture of a BBF, including the tailward return flows around the edges of the proper flow channel.

The ionospheric EISCAT VHF radar and KEV all-sky camera data indicate that a BBF channel, or the bubble, was a long elongated structure in the tail that eventually decayed starting from the Earthward end of the flow channel. The streamer orientation near the proton oval was nearly east-west, but the poleward part at higher latitudes was aligned towards the north-west direction (see e.g. Fig. 8c). When one maps the poleward- and westwardmost point of streamer 2 at 18:33 UT (indicated by a red circle in the EISCAT measurement in Fig. 8d) and the equatorward- and eastwardmost point in the ASC data to the magnetosphere by using T96 model, one obtains that those points are separated by $+4\,R_E$ in the X_{GSM} and $-4\,R_E$ in the Y_{GSM} direction. Hence, the streamer had a significant tilt in the magnetosphere, which is consistent with the direction of the corresponding BBF 2 proper flow (the Earth- and dawnward velocity components are of the same order of magnitude, see panel a in Fig. 5). The results are different from the results by Zesta et al. (2006), who mapped both east-west and north-south oriented streamers in the pre-midnight and midnight sectors and found

the orientations of the streamers to be aligned close to the X_{GSM} direction in the magnetotail.

The sharp velocity shear at the equatorward edge of the streamer suggests that the duskside return flow pattern of each BBF creates its own local flow shear in the ionosphere. In addition, the duskside return flow in the plasma sheet and in the ionosphere are associated with decreased and low plasma density (e.g. the duskside return flow in event 3a as seen both by C1 and the VHF radar). These findings are consistent with previous observations of westward ionospheric convection bursts occuring in a region of decreased electron density on the equatorward side of an auroral form and confirm suggestions of the bursts being ionospheric manifestation of BBFs (Senior et al., 2002; Zou et al., 2009).

The clear decrease in plasma density seen during the duskside tailward return flows by Cluster could be related to a formation of a depleted wake around the flanks of the moving plasma bubble. Walsh et al. (2009) have suggested that flux tubes pile up in front of the bubble, causing field-aligned plasma flow. Newly-emptied flux tubes then slip around and form a depleted wake. The return flows in events 3a and 3b, showed tailward convecting compressed flux tubes with decreased plasma density, giving support to the wake scenario. The gradual recovery of plasma density during the return flow could be then related to refilling process of the wake.

The Cluster C1 data for the first two BBF events showed the dawnward side return flow patterns. No plasma depletion was observed for these flows by Cluster, but rather increase in density (flow events 1 and 2, panels a and g in Fig. 5), which could be due to fast refilling of the depleted flux tubes in the wake. No clear ionospheric signatures of the dawnside return flow for any of the BBF-streamer events could be identified in the VHF data. However, it is possible that the return flow vectors on the poleward side (corresponding to dawnward side in the magnetosphere) of a streamer were oriented so that they were not well visible in the l-o-s velocity component measured by VHF. In addition, it is possible to argue that a part of the ionospheric poleward flows between streamers 2 and 3a would represent the dawnside return flows of BBF event 2.

During the events, the 2-D equivalent current vectors showed a northwestward directed enhanced current channel with counter-clockwise and clockwise vortices at its southwestward (dusk) and northeastward (dawn) flanks, respectively, which is the ionospheric signature of a BBF seen in equivalent currents (Juusola et al., 2009, and references therein). The orientation of the northwest current channel agree with the orientation of the streamers. Opposite to the observations of a substorm streamer by Amm et al. (1999), the equivalent currents turn 180° at the southern edge of the streamers, when they are observed close to the proton oval. That is indicative of upward field-aligned currents. If we interpret the equivalent currents to flow in the opposite direction to convection, which is a reasonable assumption for uniform conductances and on meso-scales, we deduce that for these quiet time BBFs, the convection pattern is what could be expected from the bubble model if directly mapped into the ionosphere.

The blue line in Fig. 7e is a rough estimate for the ionospheric reconnection electric field (E_r) derived from the EISCAT measurements by using the method of Vasyliunas (1984). For the electric field, a 3-min running mean has been calculated. Note the separate scale for E_r in mV m^{-1} on the right side of the panel.

The reconnection electric field is the electric field along the polar cap boundary in the rest frame of the boundary and it is a measure for the reconnection rate. It can be obtained by tracking the PCB motion and measuring the plasma flow velocity across the PCB (see e.g. de la Beaujardiere et al., 1991; Østgaard et al., 2005; Pitkänen et al., 2009a,b, for details). In this study, we have utilized both the VHF and the ESR 32 m radar data to calculate E_r. For the southward pointing ESR 32 m radar, the data covered the altitude range of 76–567 km, which corresponds to a latitude range of about 69.4–74.2° MLAT. The altitude and latitude resolutions changed from 4 km to 31 km and from ∼0.05 to 0.3° MLAT in the equatorward direction, respectively. The location of the PCB was estimated for both radars separately, from which the orientation of the boundary could be obtained.

The $\boldsymbol{E} \times \boldsymbol{B}$ plasma drift velocity was calculated by combining the ion l-o-s velocities by the two radars under the assumption that the field-aligned velocity is zero. In the calculation, the 1-min data were used for both of the radars and the VHF data was interpolated to the ESR 32 m gate latitudes. Unfortunately, poor signal-to-noise ratio for the ESR 32 m measurement at large distances (<71.9° MLAT) limited the latitude coverage from which the plasma drift velocity values could be inferred. In addition, the measurements poleward of 73° MLAT were left out from the calculation, since for the ESR 32 m radar they were from the lower F-region (150–190 km) where ion-neutral collisions may still contribute to the ion motion, or from lower altitudes. Thus, the E_r estimate could be obtained from the period of 18:07–18:47 UT when the polar cap boundary stayed within about 71.9–73.0° MLAT, which corresponds to the altitude range of about 290–190 km and 350–433 km for ESR 32 m and VHF, respectively.

The angle between the VHF and ESR 32 m radar beams was small in the current radar configuration, about 11.2° (Fig. 3), which causes uncertainty in the E_r estimation. However, the line-of-sight velocities measured by the two radars were almost aligned along the magnetic meridian, so the estimate for the north-south component of the 2-D plasma flow should be rather reliable. It can be then argued that using the 2-D plasma velocities and orientation of the boundary, we get a better estimate for the reconnection electric field than using only a single beam with the assumption that the PCB is oriented in the magnetic east-west direction and plasma flow is along the magnetic meridian.

From Fig. 7e we notice that the BBFs and associated auroral streamers appeared during a ∼35-min period after 18:16 UT, during which the ionospheric reconnection electric field E_r was enhanced (blue curve). This is consistent with the previous findings about the relation between PBIs and enhanced flux closure by e.g. de la Beaujardiere et al. (1994), Hubert et al. (2007), and Pitkänen et al. (2009a,b), and suggests that the BBFs were initiated by longitudinally localized reconnection bursts in the magnetotail. However, unlike PBIs in Pitkänen et al. (2009a,b), clear individual peaks in the reconnection electric field that could be directly associated with the corresponding BBFs are visible plausibly only for the first streamer 1, where E_r reaches a maximum of $\sim$100 mV m^{-1}.

The E_r enhancement is probably related to a change in ionospheric plasma convection due to the rotation of the solar wind IMF. As discussed in Sect. 2.1, IMF rotated to a more southward direction at the magnetospheric bow shock nose after 17:50 UT and the maximum southward IMF condition lasted from 18:00 UT until 18:16 UT, when another rotation took place (top panel in Fig. 1).

The increase in the southward IMF component indicates enhanced reconnection on the dayside magnetopause and, subsequently, increase in plasma convection. The change in ionospheric convection was indeed observed by the VHF radar at ∼18:10 UT, about 10 min after the first IMF rotation, as the equatorward l-o-s ion velocity component enhanced poleward of the PCB (Fig. 7c). Checking the l-o-s convection velocity components from several SuperDARN radars at 10-min resolution revealed that convection enhanced globally between 18:00 and 18:10 UT, and the maxima in the nightside flows were observed at about 18:20 UT (data not shown).

We suggest the following sequence of events leading to the BBFs observed. By 17:50 UT the magnetosphere had reached a quiet state (AE $\lesssim$100 nT in Fig. 1). However, the IMF had a small southward component which, together with the slowly equatorward drifting polar cap boundary in the nightside (bottom panel), indicate growth of the open flux and subsequent expansion of the polar cap caused by the low-latitude reconnection on the dayside magnetopause. The IMF rotation to a more southward direction started at 17:50 UT and IMF stayed in this direction 18:00–18:16 UT, enhancing the dayside reconnection rate and plasma convection in the ionosphere. This increased open flux transport to the nightside magnetotail. Consequently, the nightside reconnection rate enhanced, possibly locally, as the calculated reconnection electric field shows. Hence, the BBFs with associated auroral streamers resulted from reconnection bursts in the magnetotail.

4 Summary and conclusions

We have examined observations of a sequence of quiet-time Earthward bursty bulk flows on 17 October 2005. The BBFs were measured by the Cluster satellites in the evening sector near-tail plasma sheet ($X_{GSM} \sim -12$ to $-14\,R_E$). Simultaneously, high-resolution measurements were carried out by the EISCAT radars, a MIRACLE all-sky camera and magnetometers, and a meridian-scanning photometer in the conjugate ionosphere in the Scandinavian sector.

The flow events in the Cluster data showed typical signatures of Earthward BBFs, which are in accordance with the BBF plasma bubble model by Chen and Wolf (1993, 1999), e.g. deflection and compression of background plasma in front of the Earthward moving bubble, magnetic signatures of flow shear region, and the proper flows. The maximum speed of the BBF proper flows was about 400 km s^{-1}. In one case, the width of the BBF channel could be estimated to be $\sim$1.5 R_E, which is on the range of widths observed before (1–5 R_E, e.g. Nakamura et al., 2001b, and references therein).

In addition, clear evidence of tailward return flows around edges of the bubble could be seen in the Cluster data. The duskside return flows were associated with significant decrease in plasma density with a gradual recovery, which supports the recent suggestion by Walsh et al. (2009) of a wake formed by depleted flux tubes slipping tailward around the edges of the bubble. However, no plasma depletion was observed for the dawnside return flows, but rather an increase in density. We suggest that more observations of tailward return flows are needed to confirm the possible formation of a wake and to investigate the structure of the return flows.

In the ionosphere, the EISCAT VHF radar and Kevo all-sky camera made measurements of auroral streamers that can be directly connected with the corresponding BBFs observed by Cluster. In the two examples presented, the streamers started from the vicinity of the polar cap boundary, intruded equatorward, braked at 68–70° aacgm MLAT and drifted westward along the poleward edge of the proton oval, the latter measured by the Kilpisjärvi meridian-scanning photometer.

The first streamer maintained its straight orientation while drifting westward, while in the second case, the tip of the streamer intruded all the way to the equatorward boundary of the proton oval, forming a dusk-opened hook-like structure. The latter feature has been reported previously e.g. by Kauristie et al. (2003), who interpreted it as duskward diversion of the magnetotail flows related to the streamer around the more dipolar field lines.

The VHF radar measured streamers as latitudinally restricted enhanced electron temperature (T_e) bands in the F-region that detached from the polar cap boundary. A sharp velocity shear appeared at the equatorward edge of a streamer. Within the streamer itself and poleward of it, the ionospheric plasma flow had an equatorward component. The poleward flows that appeared on the equatorward side of

the streamers were associated with low electron density (N_e) and enhanced ion temperature (T_i), the latter due to frictional heating between ions and neutrals. Since we do not have a reliable estimate of the electric field within the region of increased T_i, we do not know the magnitude nor the direction of electric field. However, the situation may bear resemblance to evening sector auroral arcs, where an enhanced northward electric field is often found on the equatorward side of the arc (Aikio et al., 1993). The electrodynamics of streamers in the ionosphere is a topic of future studies.

Under uncertainties arising from the mapping (T96 model), the location and motion of the streamers and associated plasma flows in the ionosphere agree with the BBFs observed simultaneously by Cluster in the magnetosphere. This implies that the flow patterns measured by the VHF radar were the ionospheric counterpart for the BBFs in the magnetotail, including tailward return flows, in accordance with the bubble model. We suggest that each of the observed BBFs creates a plasma flow pattern in the ionosphere, in which the southeastward plasma flow within the streamer and poleward of it corresponds to the Earthward BBF channel. The duskside return flow manifests itself as a local northwestward shear flow of low density plasma on the equatorward side of the streamer. The latter agrees well with the depleted duskside return flows observed by Cluster, and is consistent with previous reports of strong westward convection bursts on the equatorward side of an auroral form at the convection reversal (Senior et al., 2002; Zou et al., 2009).

During the whole period of streamers, the meso-scale equivalent currents measured by MIRACLE magnetometers showed a pattern, which is consistent with the bubble model.

The durations of the individual streamers derived from the VHF data, in agreement with the KEV ASC and Cluster BBF data, varied between 7 and 11 min and are consistent with typical time scale of BBFs, ~ 10 min (e.g. Angelopoulos et al., 1992, 1994). The north-south cross-widths of the nearly east-west oriented streamers were $\sim$0.7–0.8° MLAT (as estimated from the VHF T_e measurements), whereas the north-south cross-widths of the ionospheric equatorward plasma flow channels, representing the ionospheric counterpart for Earthward flows of BBFs in the magnetosphere, were about 1.2–2° MLAT.

It was shown that the BBFs and associated streamers appeared during a $\sim$35-min long period, during which the reconnection rate estimated from the EISCAT data was enhanced. This period was preceded by a rotation of the IMF to a more southward direction during 25 min. Hence, we suggest that the nightside reconnection rate was elevated as a consequent of the IMF rotation and the subsequently enhanced open flux transport to the nightside.

In conclusion, we have presented the first direct high-resolution measurements linking enhanced reconnection rate in the magnetotail to formation of quiet-time BBFs and associated auroral streamers, and first simultaneous observations of BBF return flows both in the plasma sheet and in the ionosphere, in accordance with the bubble model. However, more observations of BBF-related ionospheric flows with conjugate magnetospheric measurements are still needed, in specific to study the existence of dawnside return flows in the ionosphere.

Acknowledgements. The authors thank Ritva Kuula for assistance in the EISCAT data analysis. EISCAT is an international scientific association supported by research organisations in China (CRIRP), Finland (SA), France (CNRS), Germany (DFG), Japan (NIPR and STEL), Norway (NFR), Sweden (VR), and the United Kingdom (NERC). The authors thank SPDF/OMNIWeb Plus and WDC for Geomagnetism, Kyoto, for the solar wind data and AE indices. The Cluster data were made available by FGM and CIS teams, and the CDAWEB, and the authors thank for its use. The MIRACLE network is operated and maintained as an international collaboration under the leadership of the Finnish Meteorological Institute. The authors thank PIs of the SuperDARN radars and JHU/APL for the radar data.

Topical Editor P.-L. Blelly thanks two anonymous referees for their help in evaluating this paper.

References

Aikio, A., Opgenoorth, H. J., Persson, M. A. L., and Kaila, K. U.: Ground-based measurements of an arc associated electric field, J. Atmos. Terr. Phys., 55, 797–808, 1993.

Aikio, A. T., Pitkänen, T., Kozlovsky, A., and Amm, O.: Method to locate the polar cap boundary in the nightside ionosphere and application to a substorm event, Ann. Geophys., 24, 1905–1917, doi:10.5194/angeo-24-1905-2006, 2006.

Aikio, A. T., Pitkänen, T., Fontaine, D., Dandouras, I., Amm, O., Kozlovsky, A., Vaivdas, A., and Fazakerley, A.: EISCAT and Cluster observations in the vicinity of the dynamical polar cap boundary, Ann. Geophys., 26, 87–105, doi:10.5194/angeo-26-87-2008, 2008.

Amm, O.: Ionospheric elementary current systems in spherical coordinates and their application, J. Geomagn. Geoelectr., 49, 947–955, 1997.

Amm, O. and Viljanen, A.: Ionospheric disturbance magnetic field continuation from the ground to ionosphere using spherical elementary current systems, Earth Planet. Space, 51, 431–440, 1999.

Amm, O., Pajunpää, A., and Brandström, U.: Spatial distribution of conductances and currents associated with a north-south auroral form during a multiple-substorm period, Ann. Geophys., 17, 1385–1396, doi:10.1007/s00585-999-1385-6, 1999.

Angelopoulos, V., Baumjohann, W., Kennel, C. F., Coroniti, F. V., Kivelson, M. G., Pellat, R., Walker, R. J., Lühr, H., and Paschmann, G.: Bursty bulk flows in the inner central plasma sheet, J. Geophys. Res., 97, 4027–4039, 1992.

Angelopoulos, V., Kennel, C. F., Coroniti, F. V., Pellat, R., Kivelson, M. G., Walker, R. J., Russell, C. T., Baumjohann, W., Feldman, W. C., and Gosling, J. T.: Statistical characteristics of bursty bulk flow events, J. Geophys. Res., 99, 21257–21280, 1994.

Angelopoulos, V., Phan, T. D., Larson, D. E., Mozer, F. S., Lin, R. P., Tsuruda, K., Hayakawa, H., Mukai, T., Kokubun, S., Yamamoto, T., Williams, D. J., McEntire, R. W., Lepping, R. P.,

Parks, G. K., Brittnacher, M., Germany, G., Spann, J., Singer, H. J., and Yumoto, K.: Magnetotail flow bursts: association to global magnetospheric circulation, relationship to ionospheric activity and direct evidence for localization, Geophys. Res. Lett., 24, 2271–2274, 1997.

Baker, K. and Wing, S.: A new magnetic coordinate system for conjugate studies at high latitudes, J. Geophys. Res., 94, 9139–9143, 1989.

Balogh, A., Carr, C. M., Acuña, M. H., Dunlop, M. W., Beek, T. J., Brown, P., Fornacon, K.-H., Georgescu, E., Glassmeier, K.-H., Harris, J., Musmann, G., Oddy, T., and Schwingenschuh, K.: The Cluster Magnetic Field Investigation: overview of in-flight performance and initial results, Ann. Geophys., 19, 1207–1217, doi:10.5194/angeo-19-1207-2001, 2001.

Baumjohann, W., Paschmann, G., and Cattell, C. A.: Average plasma properties in the Central plasma sheet, J. Geophys. Res., 94 , 6597–6606, 1989.

Baumjohann, W., Paschmann, G., and Lühr, H.: Characteristics of high-speed ion flows in the plasma sheet, J. Geophys. Res., 95, 3801–3809, 1990.

Birn, J., Raeder, J., Wang, Y. L., Wolf, R. A., and Hesse, M.: On the propagation of bubbles in the geomagnetic tail, Ann. Geophys., 22, 1773–1786, doi:10.5194/angeo-22-1773-2004, 2004.

Chen, C. X. and Wolf, R. A.: Interpretation of high-speed flows in the plasma sheet, J. Geophys. Res., 98, 21409–21419, 1993.

Chen, C. X. and Wolf, R. A.: Theory of thin filament motion in Earth's magnetotail and its application to bursty bulk flows, J. Geophys. Res., 104, 14613–14626, 1999.

de la Beaujardiere, O., Lyons, L. R., and Friis-Christensen, E.: Sondrestrom radar measurements of the reconnection electric field, J. Geophys. Res., 96, 13907–13912, 1991.

de la Beaujardiere, O., Lyons, L. R., Ruohoniemi, J. M., Friis-Christensen, E., Danielsen, C., Rich, F. J., and Newell, P. T.: Quiet-time intensifications along the poleward auroral boundary near midnight, J. Geophys. Res., 99, 287–298, 1994.

Grocott, A., Yeoman, T. K., Nakamura, R., Cowley, S. W. H., Frey, H. U., Rème, H., and Klecker, B.: Multi-instrument observations of the ionospheric counterpart of a bursty bulk flow in the near-Earth plasma sheet, Ann. Geophys., 22, 1061–1075, doi:10.5194/angeo-22-1061-2004, 2004.

Henderson, M. G., Reeves, G. D., and Murphree, J. S.: Are north-south structures an ionospheric manifestation of bursty bulk flows?, Geophys. Res. Lett., 25, 3737–3740, 1998.

Henderson, P. D., Owen, C. J., Alexeev, I. V., Slavin, J., Fazakerley, A. N., Lucek, E., and Rème, H.: Cluster observations of flux rope structures in the near-tail, Ann. Geophys., 24, 651–666, doi:10.5194/angeo-24-651-2006, 2006.

Hubert, B., Milan, S. E., Grocott, A., Blockx, C., Cowley, S. W. H., and Gérard, J.-C.: Dayside and nightside reconnection rates inferred from IMAGE FUV and Super Dual Auroral Radar Network, J. Geophys. Res., 111, A03217, doi:10.1029/2005JA011140, 2006.

Hubert, B., Kauristie, K., Amm, O., Milan, S. E., Grocott, A., Cowley, S. W. H., and Pulkkinen, T. I: Auroral streamers and magnetic flux closure, Geophys. Res. Lett., 34, L15105, doi:10.1029/2007GL030580, 2007.

Hubert, B., Aikio, A. T., Amm, O., Pitkänen, T., Kauristie, K., Milan, S. E., Cowley, S. W. H., and Gérard, J.-C.: Comparison of the open-closed field line boundary location inferred using IMAGE-FUV SI12 images and EISCAT radar observations, Ann. Geophys., 28, 883–892, doi:10.5194/angeo-28-883-2010, 2010.

Juusola, L., Nakamura, R., Amm, O., and Kauristie, K.: Conjugate ionospheric equivalent currents during bursty bulk flows, J. Geophys. Res., 114, A04313, doi:10.1029/2008JA013908, 2009.

Kauristie, K., Sergeev, V. A., Kubyshkina, M., Pulkkinen, T. I., Angelopoulos, V., Phan, T., Lin, R. P., and Slavin, J. A.: Ionospheric current signatures of transient plasma sheet flows, J. Geophys. Res., 105, 19417–19426, 2000.

Kauristie, K., Sergeev, V. A., Amm, O., Kubyshkina, M. V. , Jussila, J., Donovan, E., and Liou, K.: Bursty bulk flow intrusion to the inner plasma sheet as inferred from auroral observations, J. Geophys. Res., 108, A11040, doi:10.1029/2002JA009371, 2003.

Lepping, R. P., Acũna, M. H., Burlaga, L. F., Farrell, W. M., Slavin, J. A., Schatten, K. H., Mariani, F., Ness, N. F., Neubauer, F. M., Whang, Y. C., Byrnes, J. B., Kennon, R. S., Panetta, P. V., Scheifele, J., and Worley, E. M.: The WIND Magnetic Field Investigation, Space Sci. Rev., 71, 207–229, 1995.

Lyons, L. R., Nagai, T., Blanchard, G. T., Samson, J. C., Yamamoto, T., Mukai, T., Nishida, A., and Kokubun, S.: Association between Geotail plasma flows and auroral poleward boundary intensifications observed by CANOPUS photometers, J. Geophys. Res., 104, 4485–4500, 1999.

Nakamura, R., Baumjohann, W., Brittnacher, M., Sergeev, V. A., Kubyshkina, M., Mukai, T., and Liou, K.: Flow bursts and auroral activations: Onset timing and foot point location, J. Geophys. Res., 106, 10777–10789, 2001a.

Nakamura, R., Baumjohann, W., Schödel, R., Brittnacher, M., Sergeev, V. A., Kubyshkina, M., Mukai, T., and Liou, K.: Earthward flow bursts, auroral streamers, and small expansions, J. Geophys. Res., 106, 10791–10802, 2001b.

Nakamura, R., Baumjohann,W., Mouikis, C., Kistler, L. M., Runov, A., Volwerk, M., Asano, Y., Voros, Z., Zhang, T. L., Klecker, B., Rème, H., and Balogh, A.: Spatial scale of high-speed flows in the plasma sheet observed by Cluster, Geophys. Res. Lett., 31, L09894, doi:10.1029/2004GL019558, 2004.

Nakamura, R., Amm, O., Laakso, H., Draper, N. C., Lester, M., Grocott, A., Klecker, B., McCrea, I. W., Balogh, A., Rème, H., and André, M.: Localized fast flow disturbance observed in the plasma sheet and in the ionosphere, Ann. Geophys., 23, 553–566, doi:10.5194/angeo-23-553-2005, 2005.

Ogilvie, K. W., Chorney, D. J., Fitzenreiter, R. J., Hunsaker, F., Keller, J., Lobell, J., Miller, G., Scudder, J. D., Sittler Jr., E. C., Torbert, R. B., Bodet, D., Needell, G., Lazarus, A. J., Steinberg, J. T., Tappan, J. H., Mavretic, A., and Gergin, E.: SWE, a comprehensive plasma instrument for the WIND spacecraft, Space Sci. Rev., 71, 55–77, 1995.

Ohtani, S. I., Shay, M. A., and Mukai, T.: Temporal structure of the fast convective flow in the plasma sheet: Comparison between observations and two-fluid simulations, J. Geophys. Res., 109, A03210, doi:10.1029/2003JA010002, 2004.

Østgaard, N., Moen, J., Mende, S. B., Frey, H. U., Immel, T. J., Gallop, P., Oksavik, K., and Fujimoto, M.: Estimates of magnetotail reconnection rate based on IMAGE FUV and EISCAT measurements, Ann. Geophys., 23, 123–134, doi:10.5194/angeo-23-123-2005, 2005.

Pitkänen, T., Aikio, A. T., Kozlovsky, A., and Amm, O.: Reconnection electric field estimates and dynamics of high-latitude

boundaries during a substorm, Ann. Geophys., 27, 2157–2171, doi:10.5194/angeo-27-2157-2009, 2009a.

Pitkänen, T., Aikio, A. T., Kozlovsky, A., and Amm, O.: Corrigendum to "Reconnection electric field estimates and dynamics of high-latitude boundaries during a substorm" published in Ann. Geophys., 27, 2157–2171, 2009, Ann. Geophys., 27, 3007–3007, doi:10.5194/angeo-27-3007-2009, 2009b.

Raj, A., Phan, T., Lin, R. P., and Angelopoulos, V: Wind survey of high-speed bulk flows and field-aligned beams in the near-Earth plasma sheet, J. Geophys. Res., 107, 1419, doi:10.1029/2001JA007547, 2002.

Rème, H., Aoustin, C., Bosqued, J. M., Dandouras, I., Lavraud, B., Sauvaud, J. A., Barthe, A., Bouyssou, J., Camus, Th., Coeur-Joly, O., Cros, A., Cuvilo, J., Ducay, F., Garbarowitz, Y., Medale, J. L., Penou, E., Perrier, H., Romefort, D., Rouzaud, J., Vallat, C., Alcaydé, D., Jacquey, C., Mazelle, C., d'Uston, C., Möbius, E., Kistler, L. M., Crocker, K., Granoff, M., Mouikis, C., Popecki, M., Vosbury, M., Klecker, B., Hovestadt, D., Kucharek, H., Kuenneth, E., Paschmann, G., Scholer, M., Sckopke, N., Seidenschwang, E., Carlson, C. W., Curtis, D. W., Ingraham, C., Lin, R. P., McFadden, J. P., Parks, G. K., Phan, T., Formisano, V., Amata, E., Bavassano-Cattaneo, M. B., Baldetti, P., Bruno, R., Chionchio, G., Di Lellis, A., Marcucci, M. F., Pallocchia, G., Korth, A., Daly, P. W., Graeve, B., Rosenbauer, H., Vasyliunas, V., McCarthy, M., Wilber, M., Eliasson, L., Lundin, R., Olsen, S., Shelley, E. G., Fuselier, S., Ghielmetti, A. G., Lennartsson, W., Escoubet, C. P., Balsiger, H., Friedel, R., Cao, J.-B., Kovrazhkin, R. A., Papamastorakis, I., Pellat, R., Scudder, J., and Sonnerup, B.: First multispacecraft ion measurements in and near the Earth's magnetosphere with the identical Cluster ion spectrometry (CIS) experiment, Ann. Geophys., 19, 1303–1354, doi:10.5194/angeo-19-1303-2001, 2001.

Schödel, R., Baumjohann, W., Nakamura, R., Sergeev, V. A., and Mukai, T.: Rapid flux transport in the central plasma sheet, J. Geophys. Res., 106, 301–313, 2001.

Senior, C., Cerisier, J.-C., Rich, F., Lester, M., and Parks, G. K.: Strong sunward propagating flow bursts in the night sector during quiet solar wind conditions: SuperDARN and satellite observations, Ann. Geophys., 20, 771–779, doi:10.5194/angeo-20-771-2002, 2002.

Sergeev, V. A., Angelopulous, V., Gosling, J. T., Cattell, C. A., and Russell, C. T.: Detection of localized, plasma-depleted flux tubes or bubbles in the midtail plasma sheet, J. Geophys. Res., 101, 10817–10826, 1996.

Sergeev, V. A., Liou, K., Meng, C.-I., Newell, P. T., Brittnacher, M., Parks, G., and Reeves, G. D.: Development of auroral streamers in association with impulsive injections to the inner magnetotail, Geophys. Res. Lett., 26, 417–420, 1999.

Sergeev, V. A., Sauvaud, J. A., Popescu, D., Kovrazhkin, R. A., Liou, K., Newell, P. T., Brittnacher, M., Parks, G., Nakamura, R., Mukai, T., and Reeves, G. D.: Multiple-spacecraft observation of a narrow transient plasma jet in the Earths plasma sheet, Geophys. Res. Lett., 27, 851–854, 2000.

Sergeev, V. A., Liou, K., Newell, P. T., Ohtani, S.-I., Hairston, M. R., and Rich, F.: Auroral streamers: characteristics of associated precipitation, convection and field-aligned currents, Ann. Geophys., 22, 537–548, doi:10.5194/angeo-22-537-2004, 2004.

Slavin, J. A., Lepping, R. P., Gjerloev, J., Fairfield, D. H., Hesse, M., Owen, C. J., Moldwin, M. B., Nagai, T., Ieda, A., and Mukai, T.: Geotail observations of magnetic flux ropes in the plasma sheet, J. Geophys. Res., 108, 1015, doi:10.1029/2002JA009557, 2003.

Snekvik, K., Haaland, S., Østgaard, N., Hasegawa, H., Nakamura, R., Takada, T., Juusola, L., Amm, O., Pitout, F., Rème, H., Klecker, B., and Lucek, E. A.: Cluster observations of a field aligned current at the dawn flank of a bursty bulk flow, Ann. Geophys., 25, 1405–1415, doi:10.5194/angeo-25-1405-2007, 2007.

Tsyganenko, N. A. and Stern, D. P.: Modeling the global magnetic field of the large-scale Birkeland current systems, J. Geophys. Res., 101, 27187–27198, doi:10.1029/96JA02735, 1996.

Walsh, A. P., Fazakerley, A. N., Lahiff, A. D., Volwerk, M., Grocott, A., Dunlop, M. W., Lui, A. T. Y., Kistler, L. M., Lester, M., Mouikis, C., Pu, Z., Shen, C., Shi, J., Taylor, M. G. G. T., Lucek, E., Zhang, T. L., and Dandouras, I.: Cluster and Double Star multipoint observations of a plasma bubble, Ann. Geophys., 27, 725–743, doi:10.5194/angeo-27-725-2009, 2009.

Vanhamäki, H., Amm, O., and Viljanen, A.: 1-dimensional upward continuation of the ground magnetic field disturbance using spherical elementary current systems, Earth Planets Space, 55, 613–625, 2003.

Vasyliunas, V. M.: Steady state aspects of magnetic field line merging, AGU monograph on magnetic reconnection in space and laboratory plasmas, Geophysical Monograph, 30, 25–31, 1984.

Zesta, E., Lyons, L. R., and Donovan, E.: The auroral signature of earthward flow burst observed in the magnetotail, Geophys. Res. Lett., 27, 3241–3244, 2000.

Zesta, E., Lyons, L., Wang, C.-P., Donovan, E. Frey, H., and Nagai, T.: Auroral poleward boundary intensifications (PBIs): Their two-dimensional structure and associated dynamics in the plasma sheet, J. Geophys. Res., 111, A05201, doi:10.1029/2004JA010640, 2006.

Zou, S., Lyons, L. R., Nicolls, M. J., and Heinselman, C. J.: PFISR obsevations of strong azimuthal flow bursts in the ionosphere and their relation to nightside aurora, J. Atmos. Sol.-Ter. Phys., 71, 729–737, 2009.